NAVAL POSTGRADUATE SCHOOL

MONTEREY, CALIFORNIA

THESIS

REDUCTION EXPANSION SYNTHESIS FOR MAGNETIC ALLOY POWDERS

by

Samuel L. Lowell

December 2015

Thesis Advisor: Jonathan Phillips
Co-Advisor: Claudia C. Luhrs

THIS PAGE INTENTIONALLY LEFT BLANK

REPORT DOCUMENTATION PAGE			*Form Approved OMB No. 0704–0188*
Public reporting burden for this collection of information is estimated to average 1 hour per response, including the time for reviewing instruction, searching existing data sources, gathering and maintaining the data needed, and completing and reviewing the collection of information. Send comments regarding this burden estimate or any other aspect of this collection of information, including suggestions for reducing this burden, to Washington headquarters Services, Directorate for Information Operations and Reports, 1215 Jefferson Davis Highway, Suite 1204, Arlington, VA 22202–4302, and to the Office of Management and Budget, Paperwork Reduction Project (0704–0188) Washington DC 20503.			
1. AGENCY USE ONLY ***(Leave blank)***	**2. REPORT DATE** December 2015	**3. REPORT TYPE AND DATES COVERED** Master's thesis	
4. TITLE AND SUBTITLE REDUCTION EXPANSION SYNTHESIS FOR MAGNETIC ALLOY POWDERS			**5. FUNDING NUMBERS**
6. AUTHOR(S) Samuel L. Lowell			
7. PERFORMING ORGANIZATION NAME(S) AND ADDRESS(ES) Naval Postgraduate School Monterey, CA 93943–5000			**8. PERFORMING ORGANIZATION REPORT NUMBER**
9. SPONSORING /MONITORING AGENCY NAME(S) AND ADDRESS(ES) N/A			**10. SPONSORING / MONITORING AGENCY REPORT NUMBER**
11. SUPPLEMENTARY NOTES The views expressed in this thesis are those of the author and do not reflect the official policy or position of the Department of Defense or the U.S. Government. IRB Protocol number ____N/A____.			
12a. DISTRIBUTION / AVAILABILITY STATEMENT Approved for public release; distribution is unlimited			**12b. DISTRIBUTION CODE**

13. ABSTRACT (maximum 200 words)

In this work submicron scale ferromagnetic and magnetic rare-earth alloys were produced using Reduction Expansion Synthesis (RES), a technique in which metal particles are the product of the rapid heating to approximately 800 degrees Celsius, in inert atmosphere, of physical mixtures of urea, or similar molecules, and metal oxide, hydroxide or nitrates. As shown by scanning electron microscopy and x-ray diffraction, RES produced submicron magnetic particles. Essential to both 3D printing and metal injection molding (MIM) is the availability of fine powders to manufacture small, complex, metal parts. There are technological limits to the minimum particle size that can be produced using available low cost techniques, which is approximately 10 microns. This minimum particle size in turn limits the size of features on MIM and 3D printed metal parts. The demonstrated ability of RES to produce sub-micron particle sizes indicates this technology could enable the manufacture of finer features using either 3D printing or MIM.

14. SUBJECT TERMS Reduction Expansion Synthesis, 3D Printing, Metal Injection Molding, Additive Manufacturing, Permanent Magnets, Rare Earth Magnets, Ultrafine Powder			**15. NUMBER OF PAGES** 89
			16. PRICE CODE
17. SECURITY CLASSIFICATION OF REPORT Unclassified	**18. SECURITY CLASSIFICATION OF THIS PAGE** Unclassified	**19. SECURITY CLASSIFICATION OF ABSTRACT** Unclassified	**20. LIMITATION OF ABSTRACT** UU

NSN 7540–01–280–5500 Standard Form 298 (Rev. 2–89)
Prescribed by ANSI Std. 239–18

THIS PAGE INTENTIONALLY LEFT BLANK

Approved for public release; distribution is unlimited

REDUCTION EXPANSION SYNTHESIS FOR MAGNETIC ALLOY POWDERS

Samuel L. Lowell
First Lieutenant, United States Army
B.S., United States Military Academy, 2014

Submitted in partial fulfillment of the
requirements for the degree of

MASTER OF SCIENCE IN MECHANICAL ENGINEERING

from the

NAVAL POSTGRADUATE SCHOOL
December 2015

Approved by: Jonathan Phillips
Thesis Advisor

Claudia C. Luhrs
Co-Advisor

Garth V. Hobson
Chair, Department of Mechanical and Aerospace Engineering

THIS PAGE INTENTIONALLY LEFT BLANK

ABSTRACT

In this work submicron scale ferromagnetic and magnetic rare-earth alloys were produced using Reduction Expansion Synthesis (RES), a technique in which metal particles are the product of the rapid heating to approximately 800 degrees Celsius, in inert atmosphere, of physical mixtures of urea, or similar molecules, and metal oxide, hydroxide or nitrates. As shown by scanning electron microscopy and x-ray diffraction, RES produced submicron magnetic particles. Essential to both 3D printing and metal injection molding (MIM) is the availability of fine powders to manufacture small, complex, metal parts. There are technological limits to the minimum particle size that can be produced using available low cost techniques, which is approximately 10 microns. This minimum particle size in turn limits the size of features on MIM and 3D printed metal parts. The demonstrated ability of RES to produce sub-micron particle sizes indicates this technology could enable the manufacture of finer features using either 3D printing or MIM.

THIS PAGE INTENTIONALLY LEFT BLANK

TABLE OF CONTENTS

LIST OF FIGURES

LIST OF TABLES

THIS PAGE INTENTIONALLY LEFT BLANK

LIST OF ACRONYMS AND ABBREVIATIONS

EDS	Energy Dispersive X-ray Spectroscopy
FOB	Forward Operating Base
ICDD	International Centre for Diffraction Data
MIM	Metal Injection Molding
nm	Nanometers
RES	Reduction Expansion Synthesis
SCCM	Standard Cubic Centimeters per Minute
SEM	Scanning Electron Microscope
STEM	Scanning Transmission Electron Microscope
TEM	Transmission Electron Microscope
XRD	X-ray Diffraction
μm	Microns

THIS PAGE INTENTIONALLY LEFT BLANK

ACKNOWLEDGMENTS

The completion of this thesis would not have been possible without the guidance, support, and knowledge provided by my advisor, Jonathan Phillips, and my co-advisor, Claudia Luhrs. Additionally, I would like to extend a huge thank you to Sarath Menon who provided me with countless hours of guidance as I used the SEM, TEM, and XRD throughout this thesis.

THIS PAGE INTENTIONALLY LEFT BLANK

I. INTRODUCTION

A. MILITARY APPLICATION OF 3D PRINTING AND MAGNETIC COMPONENTS

In August of 2012, the United States Army deployed its first-ever fully functional mobile 3D printing lab, contained in a single shipping crate, to Afghanistan [1]. Its purpose, to enable the production of specialized components for the wide variety of equipment present on a Forward Operating Base (FOB) [1]. The Army has a massive amount of equipment deployed to remote locations throughout combat zones around the world. Each piece of equipment contains an additional long list of components, each of which may need to be replaced to keep the equipment functioning. With the creation of a mobile 3D printing lab in 2012, as seen in Figure 1, the Army was able to address its need for printable plastic components, thus enabling a reduction in the total quantity of spare components required to be stored in a FOB's inventory to ensure mission readiness.

Figure 1. The United States Army's Mobile 3D Printing Lab.

Source [1]: M. Cox, "Mobile labs build on-the-spot combat solutions," *Military. Com*, Aug.17, 2012.

However, the Army has an equally large demand for metallic components. While there are currently techniques available for 3D printing larger-sized metal components, components with smaller features require prohibitively high cost, significantly higher precision printing techniques, which are currently unattainable to wide-scale deployment throughout the Army. These small-scale components include the magnetic components widely deployed throughout the Army's radio equipment inventory [2]. These permanent magnets in the radio equipment are AlNiCo alloys, shaped to fit into the handsets as a component in the speaker [3]. Traditionally, a damaged magnet would result in the replacement of the entire handset, rather than the resupply of the individual components. Thus the Army would benefit from the ability to 3D print the magnetic speaker component as needed. To achieve this goal, not only would the army need a 3D printer capable of metal printing, but it would also need a metal powder of the right alloy composition and grain, in this case an AlNiCo magnet alloy, with a grain size small enough to accommodate the precise features of a handset's magnetic ring.

In July of 2014, the United States Navy deployed the *USS Essex* (LHD-2), the first naval ship with a 3D printer, capable of printing plastic components, permanently installed. The Navy emphasized that it was "currently in the crawl" phase of adopting 3D printing technology aboard its ships. One of the reasons the Navy is so cautious is that 3D printing has not yet reached "the point where a part printed on the [3D printer] has the same strength and overall properties that a cast part has" [4]. However, by deploying a ship with a 3D printer installed, the Navy is clearly indicating a willingness to adopt the technology at a future date.

As with the Army, the Navy also has many small magnetic components throughout a ship, components that, if damaged, would need to be replaced in order to ensure mission readiness. While the Navy does not use the same radio handsets as the Army, their radio communication techniques, used to communicate throughout a ship, all require magnetic components to function [5]. To be able to 3D print replacement magnets of the correct alloy would reduce the quantity of spare components that a navy ship would have to store. This reduction in stored parts directly benefits the stated 2015 goal

of the Navy to “promote acquisition excellence” by leveraging “strategic sourcing” by reducing the number of individual components required to be purchased [6].

As the United States Military continues to expand its reach, whether through an Army FOB located in the Afghan mountains, or a Navy submarine stationed under hostile waters for a long period of time, the need for 3D printed components becomes clear. While 3D printing plastics is already widespread and successful, there is still much room for improvement in the economical 3D printing of metal components. By demonstrating the ability to synthesize magnetic powders for use in 3D printing, this thesis will help enable additional enhancements in the way the military uses and deploys 3D printing throughout the world.

B. MOTIVATION

As previously detailed, the United States Military has begun using 3D printing in various manners. Rapid adoption of this technology will help to ensure that equipment repairs can be conducted in the fastest possible manor to ensure that soldiers, sailors, and airmen are always mission ready, especially when deployed abroad. By focusing on synthesizing magnetic powders, this thesis’ specific contribution to this goal will be in allowing for the printing of smaller magnetic components, components that exist in many forms throughout the United States Military.

C. GOALS AND OBJECTIVES

This thesis sets out to achieve two separate goals. The first goal is to demonstrate that reduction expansion synthesis (RES) is capable of producing submicron grain size powders of various metal compositions. To achieve this goal, the thesis will synthesize various metallic alloys, demonstrating not only the ability to alloy different metals through RES, but also the ability to specify the resulting alloy’s compositions through the proper determination of precursor ratio.

The second research goal is to demonstrate the synthesis of magnetic rare earth alloys. In theory, these offer a different set of challenges as compared to a pure metal alloy. The primary obstacle will be determining whether or not a Lanthanide series

element is capable of undergoing RES. If we are able to demonstrate RES using a Lanthanide series element, then the synthesis of metallic rare earth alloy powders will most likely be possible.

By attaining these two goals, this thesis will have provided new submicron metal powders for use in various industries, with direct applications to the United States Military.

II. A REVIEW OF METAL PARTICLES IN MANUFACTURING

In this chapter, several topics regarding metal particles in manufacturing are discussed. First the processes that employ metal particles including metal injection molding and 3D printing are described. Next, various commercial technologies to create metal particles are briefly outlined including crushing and grinding, atomization, and some chemical processes. These are compared with the novel technology that is the focus of this thesis, RES. This is followed by a discussion of magnetic materials, as these are the particular particles manufactured herein. Finally, some fundamentals of particle sintering are discussed as this is relevant to evaluation of the results of the RES synthesis of magnetic micron and sub-micron scale particles

A. METAL INJECTION MOLDING AND 3D METAL PRINTING

Metal injection molding (MIM) and 3D metal printing are two different methods of manufacturing small metallic components without using molten metals and casting. While MIM still uses a similar process to traditional casting, through the use of the particle injection process, the temperatures associated with the process, and therefore the energy costs, are much lower. In MIM process metal particles and a removable ‘binder are co-injected. A chemical process is required to remove the binder and heating is required to sinter the particles, but the temperature required is far below the melting temperature [7]. 3D printing metals is an entirely different process, which uses a laser and fine stream of metal to “build” the desired component [8]. To achieve this effect the laser creates a temperature, locally, equivalent or higher than that used in the MIM process.

As it pertains to magnetic material, [9] discusses the current potential for using MIM to synthesize rare earth magnets. The process used neodymium magnet powder with a grain size of 4.6 microns (μm) mixed with a wax-polymer binder as the “feedstock” material. The process then took the material and injected it into a mold, which was in turn heated to 500 degrees Celsius to remove the binding material, and then sintered at 1100 degrees Celsius. It is shown that the magnets performed nearly as well as neodymium magnets synthesized in a more traditional process.

It is hypothesized in this thesis, that the new powders created using RES, can be used in a MIM process. The advantage presented by the RES powder is that the smaller grainsize will allow for the MIM synthesis of components with smaller feature size. As explained elsewhere [10] particles used in MIM synthesis must have a grain size that is no more than five percent of the size of the synthesized components smallest feature. For example, using a 4.6 μm grain size, a particle size presently available on the market, the smallest full strength component that can be generated is approximately 100 μm or 0.1 millimeters. However, with particles on the 100 nanometer (nm) scale, as we intend to make, the smallest component size would be approximately 2 μm, two orders of magnitude smaller than possible in [9].

A difficulty of MIM as it pertains to manufacturing magnetic material is suggested in [11]. At issue is the need for the material to be manufactured within a magnetic field so that the individual particles' magnet domains will align. A device to enable magnetic alignment [11] is shown in Figure 2. The proposed schematic uses a mold surrounded by an electromagnet to create a constant field while MIM is conducted. The field aligns the magnetic domains of the individual particles involved in the MIM process, so that the final manufactured part has a homogeneous magnetic field.

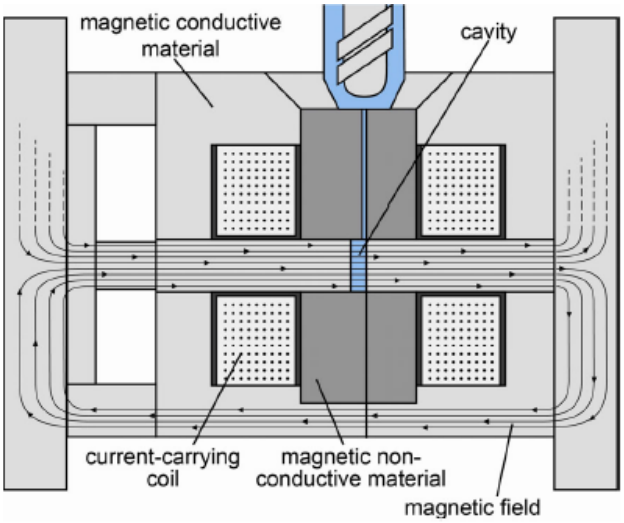

Figure 2. Proposed Schematic for MIM with Integrated Magnetic Field.

Source [11]: K. H. Kurth and D. Drummer, "Improvement of the magnetic properties of injection molded polymer bonded magnets," *2013 3rd International Electric Drives Production Conference (Edpc)*, pp. 7–11, 2013.

The other alternative manufacturing method is 3D metal printing. In [8], the process of 3D printing a metal component is described in detail. Similarly to MIM, a metal powder is required to manufacture a component. As the metal powder is deposited by the printer, a laser is used to melt the powder into place, as prescribed by a technical drawing loaded into the system's control unit. The use of the laser takes on several roles, which the article discusses in terms of the resulting metal's material characteristics.

The first type of 3D metal printing is Laser Sintering. Through this method, powder is deposited in a layer-by-layer technique. A laser sinters the powder after each layer is deposited to create a solid structure. In Laser Melting, powder is deposited layer-by-layer, much like in Laser Sintering. However, in Laser Melting, a laser is used to completely melt the layers of deposited powder, resulting in "fully dense components with mechanical properties comparable to those of bulk materials" [8]. Finally, Laser Metal Deposition is a process that works similarly to traditional 3D plastic printers. The laser melts the powder as it is deposited, eliminating the layer-by-layer step required by Laser Sintering and Laser Melting [8]. A comparison of these different methods is diagramed in Figure 3.

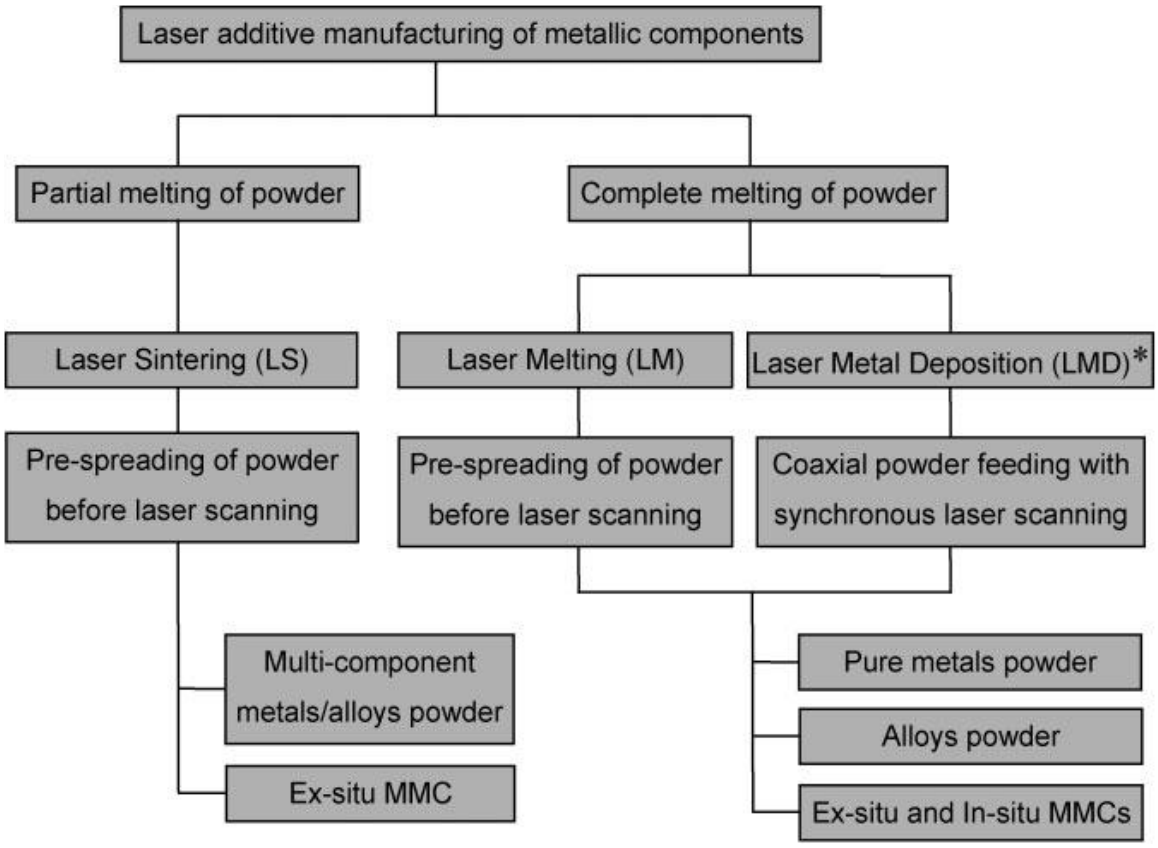

Figure 3. Differences between 3D Metal Printing Methods.

Source [8]: D. D. Gu, W. Meiners, K. Wissenbach, and R. Poprawe, "Laser additive manufacturing of metallic components: materials, processes and mechanisms," *Int. Mater. Rev.*, vol. 57, pp. 133–164, May, 2012.

Due to 3D printing's need for a metal powder, the RES technique offers a novel method of producing such a powder, especially for finer detailed 3D printing tasks. Similar to MIM, 3D printing's level of precision is a function of particle size, while also a function of the laser's spot size. Any reduction in particle size achieved by this thesis, directly lends itself to the synthesis of smaller, and finer featured components via 3D metal printing.

B. CURRENT METHODS FOR SMALL METAL PARTICLE SYNTHESIS

As noted earlier, the manufacture of metal parts with very fine features is not presently possible. Two technologies, yet to be developed, are required to allow for

smaller feature printing: i) smaller metal particle and ii) more precise high energy laser focusing. In this thesis the focus is on developing a technology that addresses one of these issues; that is RES is introduced as a means to make very small particles inexpensively. Below the various technologies presently employed to make small particles commercially are described.

1. Grinding and Crushing Methods for Powder Synthesis

Common in both MIM and 3D printing, is the demand for small particles. As the technologies currently work, the final strength of the product, as well as the precision with which the product is manufactured, are inversely proportional to grain size of the powder used in the manufacturing process. Thus, as particle size decreases, the resolution and strength of the product increases. However, smaller particle size comes at a high cost. As seen in [12], the energy, and therefore cost, required to create particles greatly increases as the desired particle size decreases [12]. Therefore, a market certainly exists for an economical submicron powder.

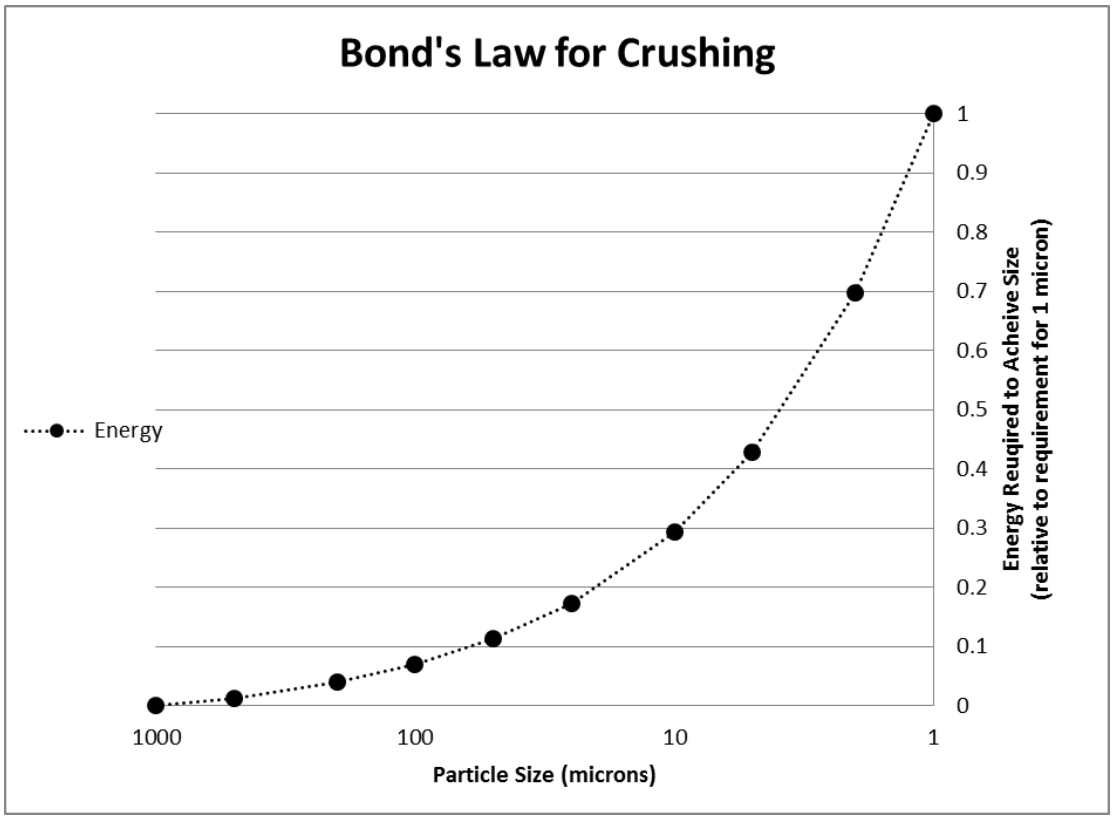

Figure 4. Bond's Law for Crushing Particles

Source [12]: W. L. McCabe, J. C. Smith and P. Harriott, *Unit Operations of Chemical Engineering.* Boston: McGraw-Hill, 2005.

As explained in [12], there is an energy cost associated with crushing particles to a desired size. The most "realistic way of estimating the power required for crushing and grinding" is to use Bond's equation: $Power = 0.3162W_i(\frac{1}{\sqrt{D_f}} - \frac{1}{\sqrt{D_i}})$, where W_i is the "work index" a constant material property that increases as the material's hardness increases, while D_i and D_f are the initial and final particle diameters respectively. This equation was used in Figure 4 to illustrate how the energy requirement to crush a particle to a specific size greatly increases as the desired particle size decreases [12]. The RES technique does not require crushing, and therefore is able to avoid the exponential energy increase when creating submicron scale particles.

2. Atomization

One of the most common methods of creating small particles for MIM and 3D printing is using atomization. As described in [13], atomization is a process where a liquid stream of metal is injected into a chamber with a fast flowing inert gas (Figure 5) which causes the stream to break up into small "atomized" particles. Atomization is capable of producing large batches of particles as small as 10 μm, with "intermetallic dispersoids" as small as 0.5 μm [13]. Atomization is a popular method of manufacturing small particles due to the consistent size distribution as well as consistent particle shape. The main drawbacks of atomization are both the natural limit on size to approximately 10 μm, and the resource intensive nature of the process. High pressure gas flow must be maintained throughout, and the metal used in the process must be heated above its melting point to be atomized.

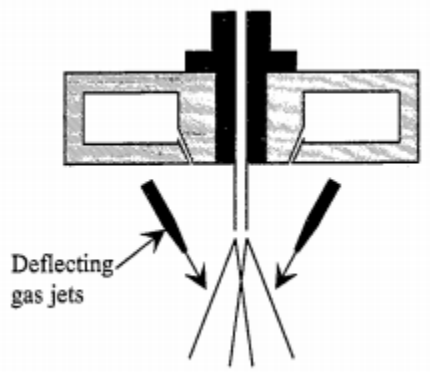

Figure 5. An Atomization Nozzle, where the Liquid Flows through the Center, and the Gas from the Sides.

Source [13]: P. Grant, "Spray forming," *Prog. Mater. Sci.*, vol. 39, pp. 497–545, 1995.

3. Jet Milling

Another method of creating small particles is through jet milling. This process uses jets of steam to force a stream of particles through a toroidal chamber at "near sonic velocity" [14]. The particles then collide with one another causing the particles to break apart into smaller particles. This process results in the smallest particles falling out of the circulating stream and concentrating in the center of the toroid where they can be collected and sorted. Commercially available jet milling (Figure 6) is capable of

achieving particle sizes as small as 37 μm, although laboratory scale jet milling has achieved particle sizes as small as 4 μm in [9]. However, Bond's equation suggests that to achieve a 4 μm powder grain size, 350% more energy is required than for the 37 μm grain size [12].

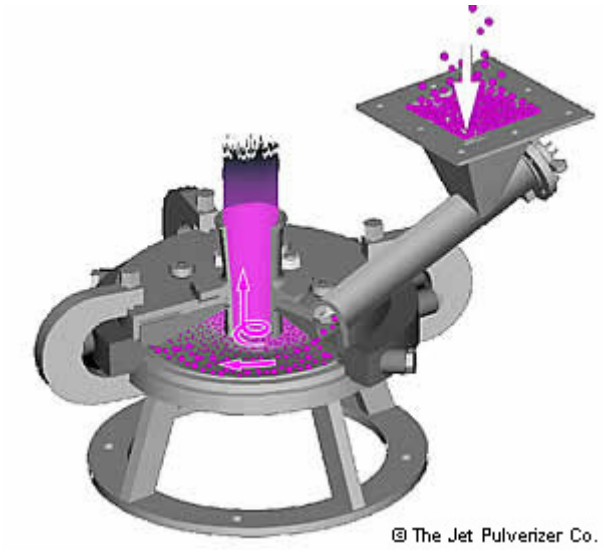

Figure 6. Jet Mill Operation Schematic

Source [14]: How Jet Mills Work - The Jet Pulverizer Company. Available: http://www.jetpulverizer.com/how-jet-mills-work.php

4. Chemical Methods of Powder Synthesis

The chemical manufacturer BASF produces a variety of proprietary carbonyl metal powders with microscale grain sizes. In [15], the powder's manufacturing process is described as thermal decomposition through the use of distillation towers to extract a specific carbonyl metal. Next, the powder is milled and treated with a proprietary coating before distribution. This reduction based process produces a variety of different particles, the smallest with an average particle diameter of 2 μm [15].

In [16], a bench scale method of producing small nickel-iron particles is described. The method used in this article was to reduce nickel and iron oxides in a hydrogen atmosphere at 600 degrees Celsius. This method is somewhat similar in conception to RES, in that it reduces precursor materials at a high temperature. However, while RES requires somewhat minimal pretreatment of the reactants, the process

described in [16] required 10 hours of milling to prepare the precursor for reduction. Thus, while [16] describes a hybrid mechanical crushing/chemical reduction process, the requirement for mechanical crushing of the powder results in the energy cost of this process being greater than a process based purely on chemical reduction.

5. Reduction Expansion Synthesis

Reduction Expansion Synthesis (RES) is a relatively new technique for the fabrication of submicron metallic particles, and the sample preparation technique used throughout this thesis [17]. In brief, the technique consists of heating a mixture of a solid reductant (e.g., urea) and a solid metal precursor in which the metal species are in a non-zero valent state (e.g., metal hydroxide, oxide, or nitrate), in an inert atmosphere (e.g., nitrogen gas). The underlying postulate is that when the solid reductant is heated to a sufficient temperature, it will decompose releasing gas phase radicals such as H, NH, NH_2, CO, etc. These species will remove oxygen species from the metal precursor, leaving zero valent metal.

In the original development of RES, as discussed elsewhere [10], [17] , only iron and nickel particles were generated. This thesis is designed to test the hypothesis that RES is a broad synthesis technique. That is, the process can be used to make a large range of metal and alloy particles, and even particles of various specific compositions. In particular, the RES process was employed herein to make both ferromagnetic alloys as well as magnetic rare-earth alloys. This thesis adapted the technique for use with both ferromagnetic alloys as well as magnetic rare-earth alloys. Additionally, this study performs additional exploration into the impact of operational parameters on particle size (see Figure 7), composition, etc.

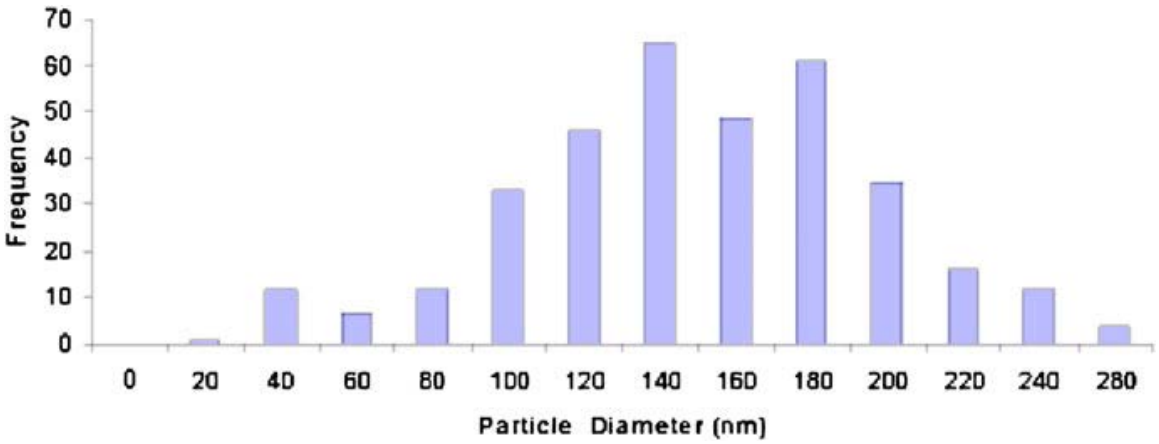

Figure 7. RES Particle Size Distribution Iron-Nickel alloy.

Source [17]: H. Zea, C. Luhrs, and J. Phillips, "Production submicron and nano metallic particles via reductive/expansion method," in *Abstracts of Papers of the American Chemical Society*, 2011.

In the 2011 article [17], the concept of RES was first introduced. The first study was limited to synthesis of submicron iron, nickel, and iron-nickel alloy particles from metal nitrate precursors and urea. The basic experimental methods to achieve success with RES were outlined. For example, from a mixture of urea and metal nitrates, metal particles only formed if the temperature was raised above the decomposition temperature for urea. The article additionally characterizes the metal particles in terms of their size distribution, indicating that the average diameter was less than 150 nm. Finally, it was suggested that the RES technique can be adapted for additional alloys, as well as graphene production [18], and that it is scalable for larger than bench scale applications [17].

Further research on the RES process [10] demonstrated that various operational parameters strongly impact the outcome of RES including the carrier gas flow rate, the urea/precursor ratio, and furnace temperature. For example, it was conclusively demonstrated that increasing the reaction temperature increases the fractional conversion of precursor to metal. Flow rate was shown to affect how complete of a reduction occurs. At lower flow rates, the "radical" reducing species generated by the decomposition of the urea gas are resident in the area of the metal precursor components for a longer period. This increases the net reaction, hence permitting more metal to form. Put another way:

High flow rates flush the reducing species out of the reactor before they have time to react with metal precursors. It is also shown that the urea to precursor ratio controls how much carbon is deposited onto the metal product. At higher ratios (10:1), significantly more carbon is present in the final product than at lower ratios (5:1). In that study, only two urea-to-precursor ratios were studied, thus, further experimentation is necessary to find the precise ratio to maximize the fractional conversion of the precursors, while minimizing the amount of carbon deposition on the metal powder product. While this article focused primarily on metal oxides and hydroxides as precursors, the conclusions it draws about the conditions under which RES is performed likely apply to metal nitrate precursors as well [10].

Additional work has been done to expand RES to wider applications. In [18], RES was used to reduce graphite oxide in order to produce graphene sheets. This study demonstrates the ability to use RES with non-transition metal elements, and demonstrates its capabilities as a method of reducing many different precursors.

Overall, the literature currently available on RES, suggests that optimal experimental conditions, for the synthesis of metal alloys, include a temperature no less than 800 degree Celsius, a urea to precursor ratio of 5:1 or less to ensure minimal carbon formation, and a nitrogen flow rate of less than 14 square cubic centimeters per minute. Additional work can be conducted to test the hypothesis that this process is scalable, and comparisons can be made between RES and current industrial best practices to form submicron scale metal particles. This thesis tends to explore both of these areas, while also expanding the list of alloys successfully synthesized through the use of RES.

C. MAGNETIC ALLOYS AND POWDER CHARACTERISTICS

In this section, a survey of current literature on a variety of topics significant to this thesis is conducted. An overview of ferromagnetic alloys is provided, with the various alloys discussed in detail. Additional information is provided on the more modern rare-earth magnetic alloys, and their improvements and limitations relative to ferromagnetic alloys. Finally, powder characteristics are discussed in terms of the types of agglomeration essential to this thesis.

1. Ferromagnetic Alloys

Ferromagnetic Alloys are a class of magnetic consisting of iron, nickel, aluminum, and cobalt [19]. These metals are alloyed together to create magnetic alloys of varying strengths. This section discusses a special class of ferromagnetic alloys known as AlNiCo alloys, and also surveys the other types of ferromagnetic alloys.

The first class of ferromagnetic alloys is permanent or hard magnets. Discussed in [20] the AlNiCo alloys are a variety of alloys containing the ferromagnetic metals, as well as small percentages of niobium, copper, and titanium. The specific composition is identified by the number following the AlNiCo name, for example an AlNiCo 5 alloy contains 8% aluminum, 14% nickel, 24% cobalt, 3% copper, and 51% iron [21]. AlNiCo alloys are permanent magnets, meaning that they have a high retentivity, or tendency to hold their magnetism when removed from a magnetic field. The article proposes that certain AlNiCo alloys are even capable of replacing rare-earth magnets (more information on magnetic rare earth alloys is contained in the next section) in certain high temperature applications, as the cost of certain rare earth magnets increases [20], [22]. Additional work in [23] explains the interaction of the various alloying constituents of AlNiCo magnets in terms of their tendency to enable permanent magnetism.

The second class of ferromagnetic alloys is known as soft magnets. Soft magnets align their magnetic domains when in the presence of an external magnetic field, but tend to lose their magnetism when removed from the magnetic field, thus having a low retentivity. A variety of nickel-iron/cobalt compositions are used in aerospace, industrial engineering, electronics, the automotive industry, and the electrical industry to create low cost soft magnetic alloys [24]. Trade-offs in terms of cost/performance determines which are appropriate for particular applications. For example, cobalt-nickel alloys provide better performance in high temperature and corrosive environments, but at a higher cost than other soft magnets [24].

As a class of magnetic material, ferromagnetic alloys offer a wide range of uses throughout industry. Their use as both permanent and soft magnets suggests that a successful manufacturing technique for various ferromagnetic alloys will have implicit

value in several different sectors of industry. The targeted alloy compositions for the work performed for this thesis encompass both the permanent and soft types.

Another feature of the present work that is significant in terms of applications: small particle size. Many magnets are very small and shaped for particular applications. Often, magnets of this type are not made by machining larger metal for two reasons. First it is wasteful as material removed during machining must be reprocessed. Second, machining is relatively slow, hence expensive. Thus, many small magnets are created by a type of molding process, called particle injection molding. In this process, particles and binder, and sometimes "wax," are injected into a mold. The material is heated to create sintered metal, and at some stage the wax dissolves. Binders, like nylon, sometimes remain to create flexible magnets. In order to make small, smooth parts the "particle size" must be no more than 10% of the smallest feature size. Hence, smaller particles enable smaller "features."

2. Magnetic Rare-Earth Alloys

Magnetic rare-earth alloys are a class of materials consisting of magnetic alloys made from rare-earth elements. The two most common types of rare-earth magnets are samarium-cobalt magnets and neodymium magnets [20]. Neodymium magnets have been gaining in popularity lately due to their lower cost relative to the older samarium-cobalt magnets. However, neodymium magnets have a low Curie temperature, which is the temperature at which they lose their magnetic strength [20]. Due to known limitations in RES, the neodymium based magnets were not explored in this thesis. As a result, this section focuses on background information about the synthesis and use of samarium-cobalt magnets.

Samarium-cobalt magnets are derived from two different alloys of samarium and cobalt, $SmCo_5$ (1:5-type) and Sm_2Co_{17} (2:17-type). These two alloys tend to offer very similar magnetic characteristics, with the 2:17-type demonstrating slightly better retentivity [25]. There have been many efforts undertaken to synthesize samarium-cobalt nanoparticles [26], generally using a wet lab approach, to reduce samarium and cobalt compounds to form a 1:5-type alloy. Their resulting product is an agglomeration of

1:5-type alloy and pure cobalt metal. However, the process requires several steps and many hours to complete as the solutions must be treated at various high temperatures and centrifuged to extract the 1:5-type alloy from the solvents used in the process [26].

Another wet lab approach to synthesizing samarium-cobalt particles is described in [27]. This process was completed using samarium and cobalt salts in a deoxygenated water solution. The resulting particles were then annealed to the point that they were approximately 40 nm in diameter. This process is an improvement from the previous paper in terms of time required to synthesize the nanoparticles, however the process still takes over 6 hours, with additional time required to extract the final product [27].

3. Particle Distributions and Agglomeration

When analyzing particles on the submicron scale, a consideration must be made for how they tend to agglomerate. With traditional metal powder particles, a common method of agglomeration is through sintering, which creates “necks” between particles. Sintered particles can be seen in Figure 8. where a set of particles were observed as they were sintered. Sintering is a thermal process, at a point close to, but below, the melting temperature of the metal powder. The result is that the particles in a powder agglomerate to form a bulk material, separated via by “necks” [28].

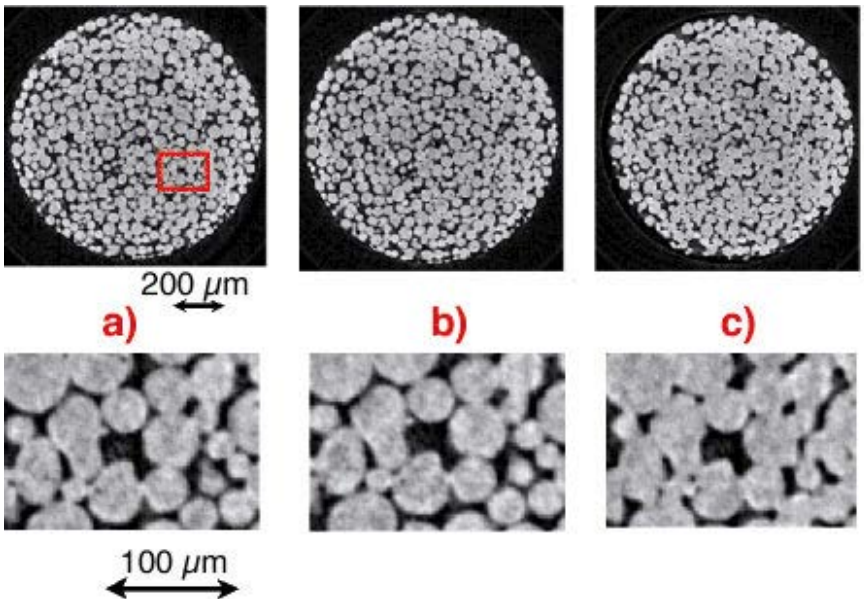

Figure 8. Copper Particles a) Pre-sintering, b) Post-sintering at 1000° C, c) Post-sintering at 1050° C

Source [28]: *In situ Microtomography Study of Metallic Powder Sintering*. Available: http://www.esrf.eu/UsersAndScience/Publications/Highlights/2002/Materials/MAT3

When dealing with magnetic powder particles, an additional form of agglomeration occurs due to the magnetic characteristics of the particles. This agglomeration results from the magnetic poles of particles attracting to one another and the agglomeration takes on more linear profile as seen in Figure 9. The linear agglomeration caused by the magnetic forces is not as permanent as agglomeration from sintering [29], [30]. A second form of magnetic agglomeration exists when a ferromagnetic material is exposed to a magnetic field. This externally induced magnetism results in particles becoming more ordered as the applied magnetic field strength is increased [31], [32].

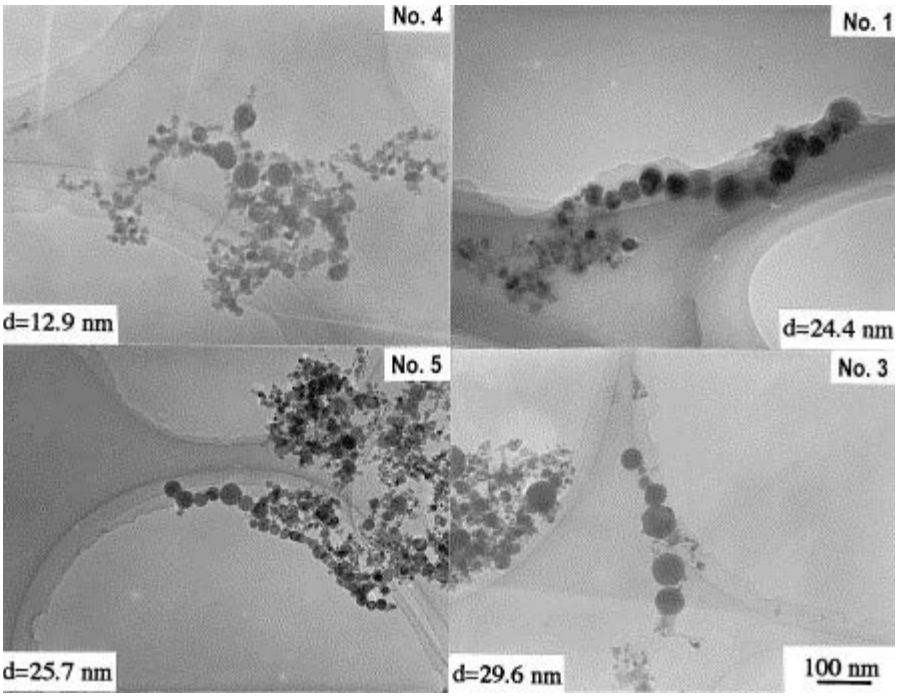

Figure 9. Magnetic Agglomeration of AlNiCo Alloys

Source [29]: X. Li, A. Chiba, M. Sato, and S. Takahashi, "Synthesis and characterization of nanoparticles of Alnico alloys," *Acta Mater.*, vol. 51, pp. 5593–5600, Oct. 20, 2003.

Magnetic agglomeration is an important phenomenon to understand when analyzing potentially magnetic powders, as it is a simple method for detecting magnetically active particles using basic SEM and TEM imaging techniques.

III. EXPERIMENTAL METHODS

In this chapter, the experimental methods used to synthesize and characterize the materials created with the Reduction Expansion Synthesis (RES) method are discussed in detail. The first section reviews the experimental process used to prepare precursors for, and conduct, RES. This includes several steps using basics laboratory skills as well as some technical work in operating a bench top tube furnace. The second section describes the various characterization techniques used to analyze the materials produced via RES, including X-Ray Diffraction (XRD), Scanning Electron Microscopy (SEM), Transmission Electron Microscopy (TEM), Scanning Transmission Electron Microscopy (STEM), and Energy Dispersive X-Ray Spectroscopy (EDS).

A. SYNTHESIS

The following section breaks down the process used to synthesize nanoscale magnetic particles using RES.

1. Preparation of Precursors

In order to prepare the precursor materials for RES, the various metal nitrates and urea were physically mixed in a prescribed mass ratio. For this thesis nickel (97% nickel nitrate hexahydrate, Sigma Aldrich), iron (98% iron nitrate nonahydrate, Sigma Aldrich), cobalt (98% cobalt nitrate hexahydrate, Sigma Aldrich), samarium (99.9% samarium nitrate hexahydrate, Sigma Aldrich), and aluminum (aluminum nitrate nonahydrate, Alfa Aesar) precursors were all used with the RES technique to synthesize a variety of nanoscale magnetic particles. Additionally, laboratory grade urea pellets (99.5% urea, Sigma Aldrich) were used, with a 2:1 urea to metal nitrate mass ratio. Below is a sample table to illustrate the methods used for determining the correct masses of precursors to synthesize a specific metal alloy, where the tan blocks reflect manually entered fields, and the blue boxes are the outputs:

Table 1. Calculations for RES Precursors

Experiment:	Sm2Co17	Molar Mass	Metal Molar Mass	wt% of Final Products
Precursor 1:	Co(NO3)2.6H2O	291.03	58.9332	0.769135881
Precursor 2:	Sm(NO3)2	444.47	150.36	0.230864119
Urea Mass:	1	Urea Mass Ratio:	2	
Precursor Ratio	Experimental Mass	Expected Final Metal Mass		
3.79822605	0.423845831	0.085828235		
0.682443303	0.076154169	0.025762236		
Total Precursor Mass:	0.5			

After the precursor materials were properly measured, they were placed together in a single batch for mixing, as seen in Figure 10.

Figure 10. Metal Powder Precursors in Mortar Prior to Mixing

The precursor materials were then vigorously ground to a homogeneous powder with a mortar and pestle. Grinding produced a homogeneous slurry. The resulting slurry (Figure 11) was then spread into an alumina boat, which in turn was placed into a quartz tube where the RES process would take place.

Figure 11. Precursor Slurry in Alumina Boat for Heating

2. Tube Furnace Operation

After sealing off both ends of the quartz tube containing the urea and metal nitrate mixture, 99.999% Nitrogen gas was flowed through the quartz tube at 100 standard cubic centimeters per minute (sccm) for thirty minutes. During this time, the quartz tube was placed into a Thermo Scientific Lindberg Blue M tube furnace, and the furnace was preheated, at a location downstream from the alumina boat, to 800 degrees Celsius, as seen in Figure 12.

Figure 12. Furnace Arrangement, Prior to Heating Sample

At the conclusion of the thirty minutes of nitrogen flow, the nitrogen flow rate was reduced to 10 sccm, and the quartz tube was moved so that the alumina boat containing the urea and metal nitrate mixture was in the center of the preheated furnace.

The furnace was then allowed to reheat to 800 degrees Celsius, a process that usually took between three and four minutes to complete. At the conclusion of this reheat process, the quartz tube was repositioned so that the furnace heating element was downstream from the alumina boat. This led to very rapid cooling of the material in the alumina boat. As soon as the boat was removed from the furnace, the nitrogen flow rate was increased back to 100 sccm, in order to quickly cool the sample. When the furnace reached a temperature below 200 degrees Celsius, the quartz tube and alumina boat were removed from the furnace, and allowed to cool in open air, until reaching room temperature.

The alumina boat was then removed from the quartz tube, and the material inside the alumina boat, as seen in Figure 13, was collected for characterization.

Figure 13. Alumina Boat with Powder Sample following RES

B. CHARACTERIZATION

When analyzing and determining the physical properties of any micro or nanoscale sample, several different characterization techniques are used. For a sample produced through RES, the main characterization techniques are SEM, TEM, EDS, and XRD analysis, additional size analysis was conducted using ImageJ software. In this section, the specifics of each of these techniques will be discussed in detail.

1. Scanning Electron Microscope

The scanning electron microscope, or SEM, is an instrument commonly used to analyze conductive samples on the micro and nanoscale. The instrument uses an electron beam to map the surface of a sample and renders an image resembling an optical microscope's output, except in grayscale with greater depth of field. As it pertains to this thesis, all SEM work was conducted using a Zeiss Neon 40 Field Emission Scanning Electron Microscope, as seen in Figure 14.

Figure 14. Zeiss Neon 40 Field Emission Scanning Electron Microscope

Samples were prepared for the SEM using two different methods. The first method was to create a "dry" sample, where the powder was applied directly to the SEM stub and placed in a vacuum. The "dry" samples allowed for analysis of the RES product as it appears immediately following RES, and without any additional treatments or processing. The "dry" method can be seen on the right stub in Figure 15. The second method was to create a "wet" sample, where the powder was dispersed in an ethanol

solution (99.5% ethanol, Sigma Aldrich) using a Branson 2510 Sonicator for 30 minutes prior to being pipetted onto the SEM stub and allowed to dry. The “wet” method was used to analyze the RES product’s particle size, and determine how easily dispersed the RES product is for the purpose of creating powders with a grain size on the nanoscale. The “wet” method can be seen on the left stub in Figure 15.

Figure 15. SEM Samples Stubs prepared for Analysis. “Wet” Preparation (left) and “Dry” Preparation (right) are Both Shown in this Image

In both methods, the SEM stubs were left in a vacuum for no less than twelve hours to prepare them for analysis. The SEM stubs were next transferred to the SEM chamber for analysis. The standard conditions for analysis were an accelerating voltage of 20 kilovolts, and an aperture size of 30 μm. The resulting image is produced in greyscale and can be seen in Figure 16.

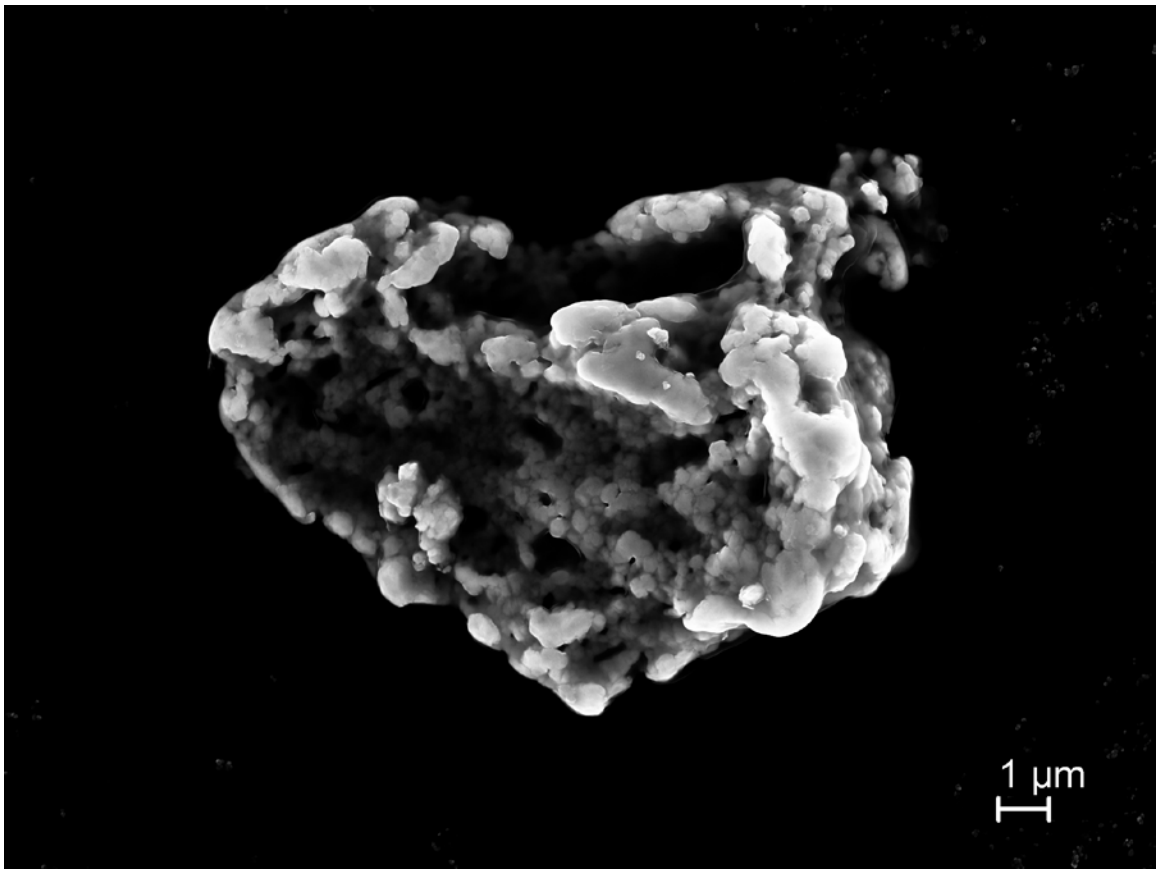

Figure 16. SEM Image of Fe-78wt%Ni at 20 kV and 5,000x Magnification

2. Transmission Electron Microscope

The transmission electron microscope, or TEM (see Figure 17), uses optical microscopy principles to create an image using a beam of electrons in place of a beam of light. While the SEM creates an image based on reflected electrons, the TEM creates images based on electrons that have passed through a sample. An additional difference between SEM and TEM is that while the SEM scans the sample, the TEM produces its entire image at once, with a spot size manipulated by the operator. Due to the very short wavelength of the high energy electrons employed in TEM, angstrom level resolution can be achieved, which is approximately 100 times higher resolution than the SEM. Another component of TEM analysis is the use of Scanning Transmission Electron Microscopy, or STEM. STEM is the process of focusing the TEM's beam to an extremely small spot size, and then scanning the sample using the beam to map the surface of the sample.

STEM is similar to SEM in this manner, because both methods scan the sample to create the image. The TEM analysis of the RES samples was conducted using an FEI TEM, with STEM capabilities built into the system.

Figure 17. FEI Transmission Electron Microscope

TEM samples are prepared in a method similar to the “wet” SEM samples as discussed in the SEM section. The sample powder to be analyzed is dispersed in an ethanol solution and sonicated for 30 minutes [33]. The resulting solution is pipetted onto a copper grid, and the grid is then placed into the TEM column under vacuum. Once in the TEM, the sample must be aligned with the electron beam operating at an accelerating voltage of 200 kilovolts. The alignment is controlled by a magnetic lens and an aperture

allowing the operator to focus the beam and control the spot size on the sample. The system is then able to produce extremely high magnification images, such as the one in Figure 18.

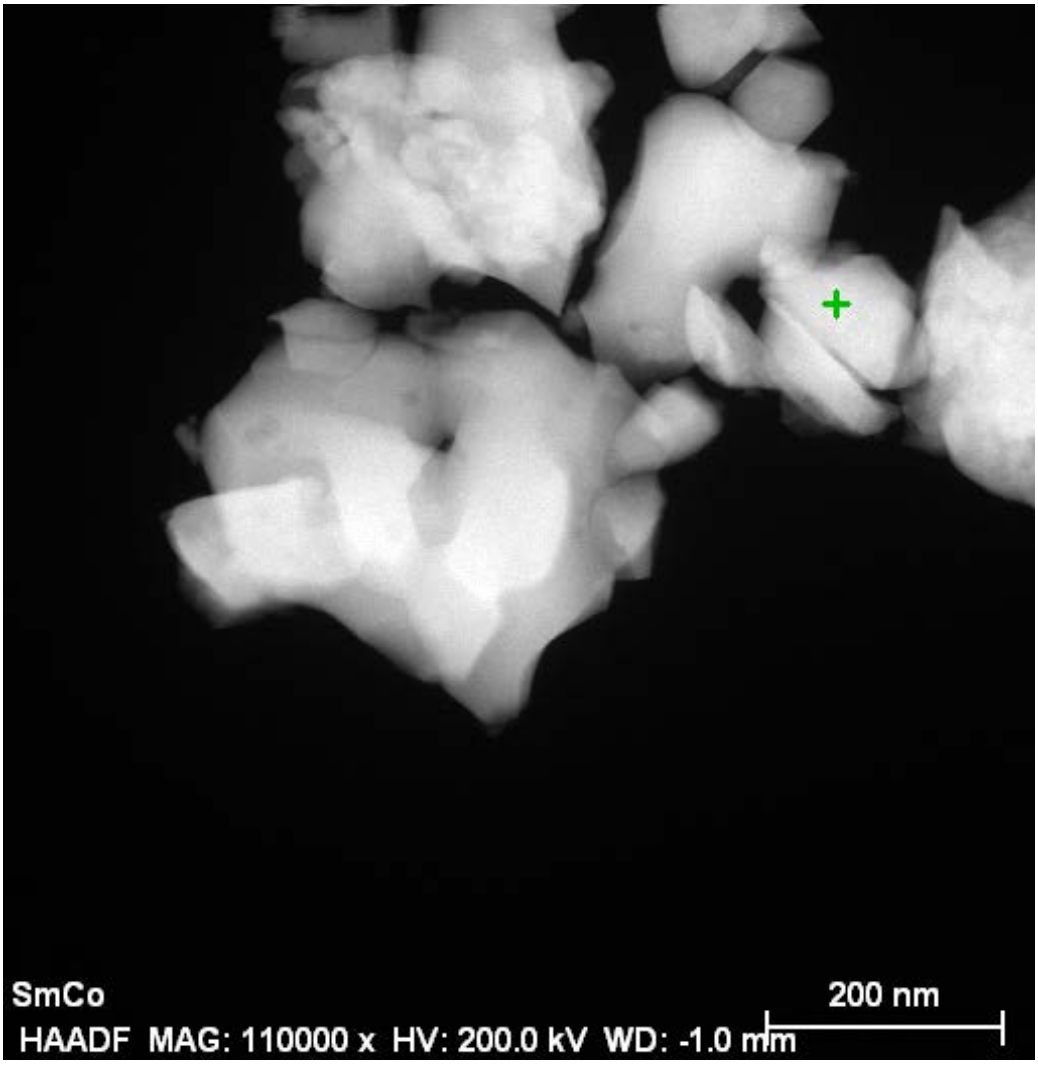

Figure 18. Samarium-Cobalt Powder as Imaged Using STEM at 200kV and 110kx Magnification

3. Energy Dispersive X-Ray Spectroscopy

Energy Dispersive X-Ray Spectroscopy, also known as EDS, was used in conjunction with both the SEM and TEM. EDS is a method of determining the elemental composition at the surface of a sample. The EDS operates by detecting the x-ray energy

produced by a displaced electron in an atom struck by the high voltage electron beam found in both the SEM and TEM. Every element has its own characteristic x-ray energies, which EDS is able to detect, and associate with a specific location on the image of a sample. This allows for not only the collection of composition over an area, but also precise composition maps of a sample's surface. A spectrum is produced with peaks associated with the x-ray energy of the atoms contained within a sample. For this research, and EDAX EDS system was used with SEM analysis, while a Bruker EDS system was used with STEM analysis.

4. X-Ray Diffraction

X-Ray Diffraction, also known as XRD, is essentially the instrumental implementation of Bragg's Law. The law, which states: $2d\sin\theta = n\lambda$, where d is the distance between atoms in a crystalline structure, θ is the angle of incidence, or the angle at which the x-ray beam is striking the sample, n is a positive integer associated with the peak number, and θ is the wavelength of the x-ray beam. Since the distance between atoms in a crystalline structure is unique, Bragg's law can be used to identify this distance, and therefore the chemical composition of a sample, given that the sample has a crystalline structure and the x-ray wavelength and incident angle are known. Using the XRD, the x-ray wavelength, and incident angle are both known variables throughout the experiment, thus the determination of a samples chemical composition is made possible. An example spectrum can be seen in Figure 19.

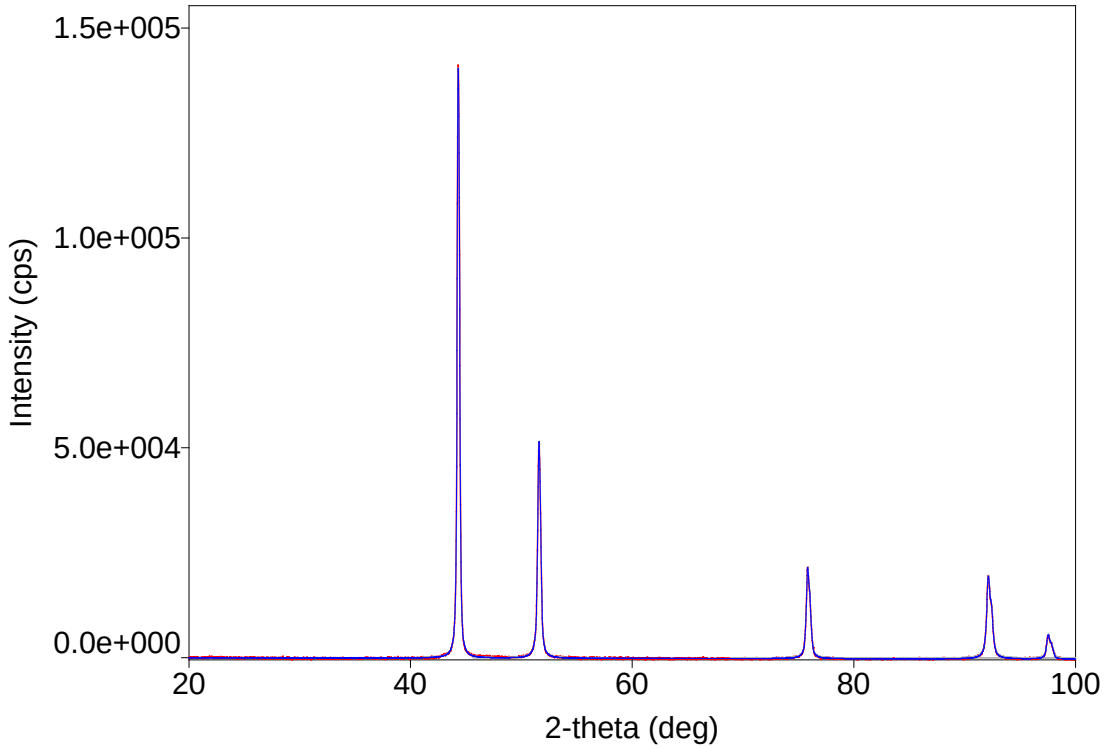

Figure 19. Example XRD Spectrum

The XRD characterization of the RES samples was conducted using a Rigaku XRD (see Figure 20), with analysis conditions set at 40 kV and 15 mA using a copper x-ray source with a wavelength of 1.56 Angstroms. The angular scan rate was changed for practical reasons, for example, when trying to identify a sample of pure metallic iron, the angular scan rate of the XRD can be accelerated due to the highly crystalline nature of the sample producing minimal to no noise in the spectrum. However, if the iron was part of an amorphous compound, the XRD's angular scan rate would need to be reduced in order to eliminate increase the signal to noise ratio and create clearly defined peaks.

The XRD samples were prepared by placing fine powders, produced using RES, on an XRD sample holder, so that the surface of the powder is level with the edges of the sample holder, a process which ensures proper sample alignment. The XRD then spins the sample in place while rotating the sample on an axis perpendicular to the incident x-ray beam. The rotation allows for the incident x-rays to strike the sample at all potentially relevant angles.

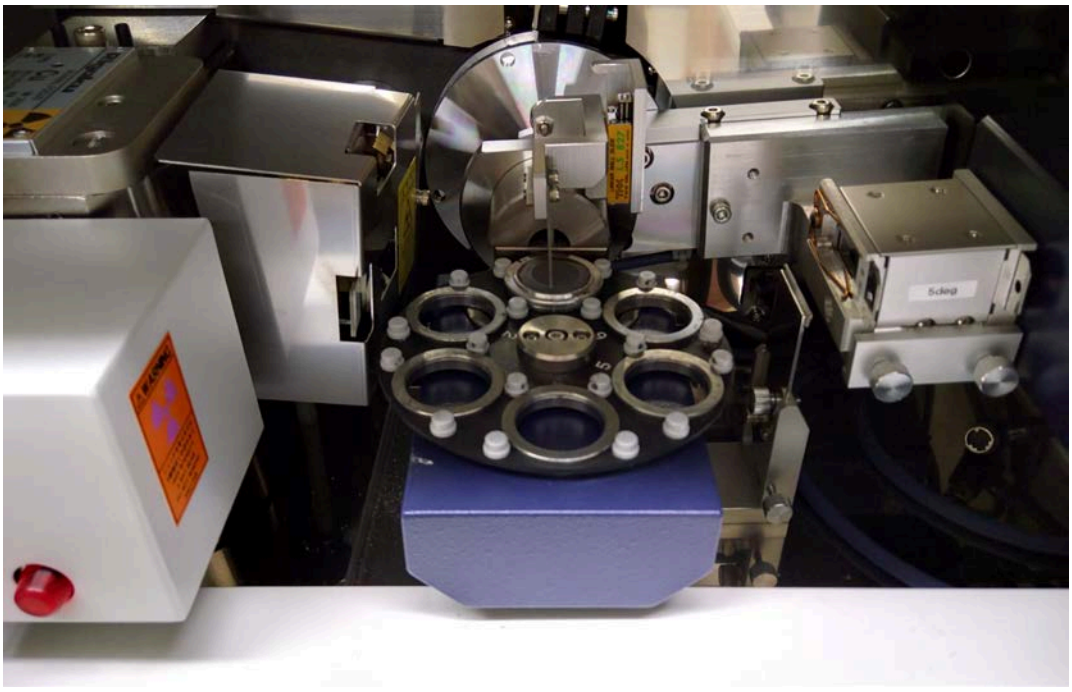

Figure 20. XRD Apparatus, the X-Ray Source is on the Right Side of the Image, the Samples Are Placed on the Numbered Tray in the Center.

XRD spectra were then compared to the International Centre for Diffraction Data's (ICDD) database of cards specifying expected peak locations for all well-known compounds. Analysis of the spectra was performed using PDXL software from Rigaku to assign the various peaks found using the XRD to the known peaks from the ICDD database.

5. Statistical Characterization Methods

In order to characterize the particle size distribution of the various powders produced through RES, ImageJ software was used. ImageJ is an open source Java based image analysis software [34]. Using ImageJ, a large quantity of particles can be measured in a timely manner. This thesis employed ImageJ to create particle size distributions by analyzing the SEM images associated with the "wet" dispersed powder samples. [35] was used as a standard operating procedure to ensure consistent particle size analysis. The data produced by ImageJ was then analyzed using R, an open source statistical analysis software.

IV. RESULTS AND DISCUSSION

This section will break down the results into two portions. The first portion of the results describes the analysis of transition metal based ferromagnetic alloys produced in this work. In particular, the analysis of materials generated in efforts to produce both hard and soft AlNiCo magnet powders is presented. The second portion of the results assesses the success of efforts to synthesize magnetic rare earth alloys. The analysis of the rare earth metals includes additional work to identify whether or not a Lanthanide series element is amenable to successful treatment with RES.

In both sections, an attempt was made to determine: the chemical composition of the material and the particle size distribution of the material. The former employed XRD and EDS, while the latter required statistical analysis of the SEM and TEM imagery produced throughout this thesis.

A. FERROMAGNETIC POWDER SYNTHESIS

1. Composition Determination with EDS and XRD

In performing the RES experiments, several ferromagnetic compositions were selected, as shown in Table 2. The calculations in Table 1 were then used to determine the proper amount of precursors to achieve the intended compositions through RES. In order to verify that RES not only reduced the precursors, but also facilitated alloying in the proper composition, XRD and EDS analysis were used to check both the composition of the material, and the atomic structure of the material.

Table 2. Target Compositions of Ferromagnetic Powder Experiments

Name	wt% Al	wt% Ni	wt% Co	wt% Fe
Fe-50wt%Ni	0	50	0	50
Fe-78wt%Ni	0	78	0	22
Co-50wt%Ni	0	50	50	0
AlNiCo-5	8	14	24	54

a. Fe-78wt%Ni

EDS analysis was used to determine the bulk powder composition of the iron-nickel powder produced using RES. The resulting composition is shown in Table 3. The synthesized powder's bulk composition is extremely close to that of Fe-78wt%Ni. However, further analysis of atomic structure through XRD is necessary to ensure that the powder is indeed an alloy rather than a mixture of pure nickel and pure cobalt powders.

Table 3. Iron-Nickel Powder EDS Results

Element	Wt%	At%
Fe	19	20
Ni	81	80

Further XRD analysis in Figure 21 shows only a single peak at 44 degrees angle. This is indicative of a single phase being present, and therefore suggests an iron-nickel alloy is the only phase in the powder. Had the XRD results shown two distinct peaks around 44 degrees that would suggest a segregated powder containing both nickel particles and iron particles. Instead, the presence of a single peak, in combination with the EDS determined bulk composition; suggest that RES successfully produced a Fe-78wt%Ni powder.

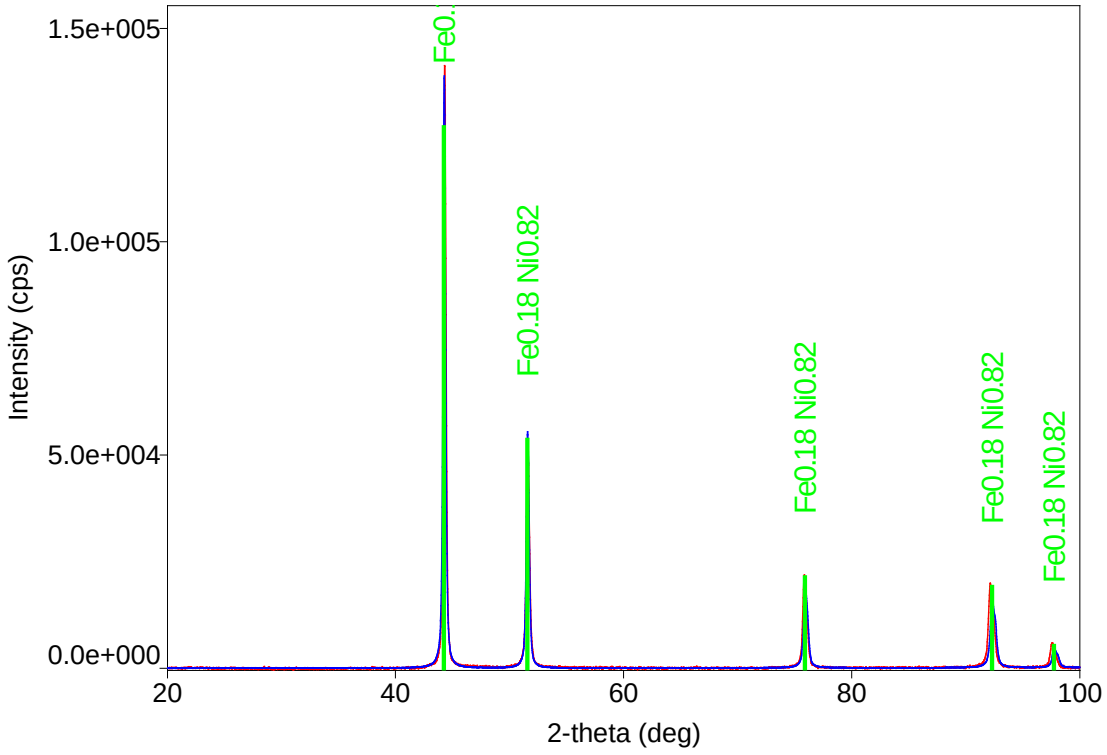

Figure 21. XRD Spectrum for Iron-Nickel Powder

b. Fe-50wt%Ni

EDS analysis was used to determine the bulk powder composition of the iron-nickel powder produced using RES. The resulting composition is shown in Table 4. The synthesized powder's bulk composition is extremely close to that of Fe-50wt%Ni. However, further analysis of atomic structure through XRD is necessary to ensure that the powder is indeed an alloy rather than a mixture of pure nickel and pure cobalt powders.

Table 4. Iron-Nickel Powder EDS Results

Element	Wt%	At%
Fe	47	48
Ni	53	52

Further XRD analysis in Figure 22 shows only a single peak at 44 degrees. This is indicative of a single phase being present, and therefore suggests a iron-nickel alloy is the only phase in the powder. Had the XRD results shown two distinct peaks around 44 degrees that would suggest a segregated powder containing both nickel particles and iron particles. Instead, the presence of a single peak, in combination with the EDS determined bulk composition; suggest that RES successfully produced a Fe-50wt%Ni powder.

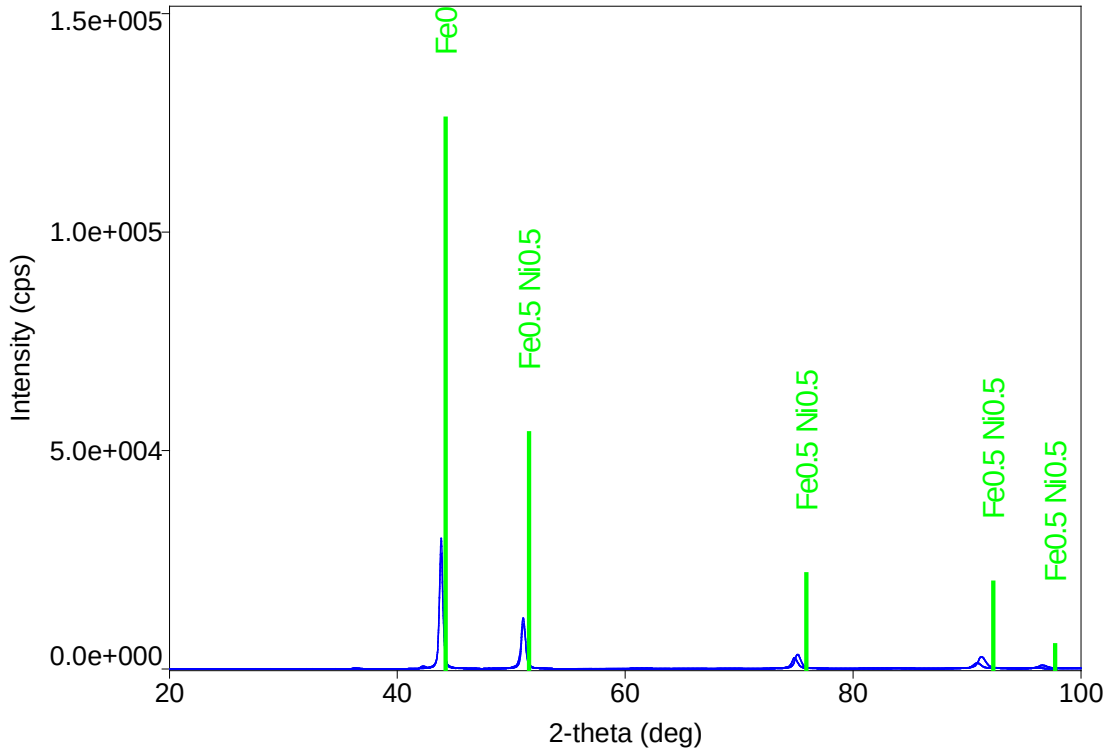

Figure 22. XRD Spectrum for Iron-Nickel Powder

In order to ensure that only one phase is present in each spectrum, it is important to analyze the area around a single peak on the XRD. Figure 23 shows the 44 degree peaks of both phases of iron-nickel powder, as well as the cobalt-nickel powder, which will be discussed in the next section. The peaks in the figure are labeled according to which sample they are from. Since each sample has one smooth and distinct peak, it can be concluded that each sample consists of one phase of either iron-nickel or cobalt-nickel.

This result suggests that not only is RES capable of producing a variety of alloys, but that precursor ratios effect and determine the phase produced through RES.

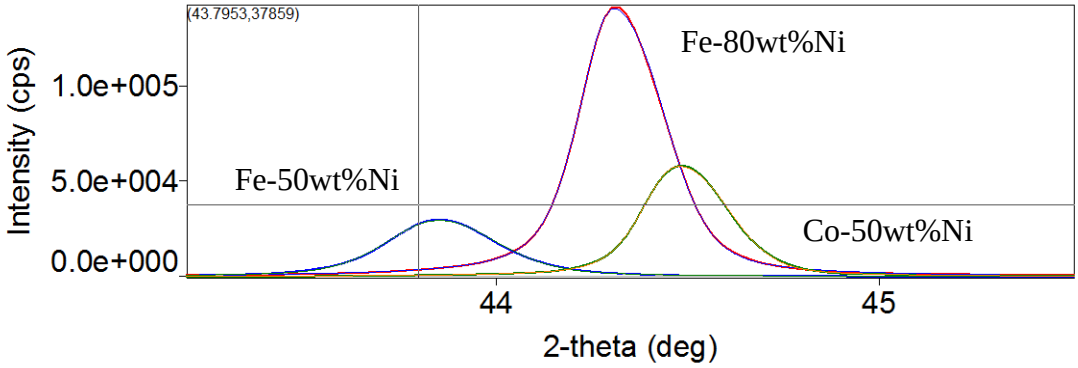

Figure 23. XRD Spectra for Both Iron-Nickel Compositions as well as the Cobalt-Nickel Composition on the Same Plot

c. Co-50wt%Ni

EDS analysis was used to determine the bulk powder composition of the cobalt-nickel powder produced using RES. The resulting composition is shown in Table 5. While there is a small amount of oxidation present, the synthesized powder's bulk composition is extremely close to that of Co-50wt%Ni. However, further analysis of atomic structure through XRD is necessary to ensure that the powder is indeed an alloy rather than a mixture of pure nickel and pure cobalt powders.

Table 5. Cobalt-Nickel Powder EDS Results

Element	Wt%	At%
Co	51	50
Ni	49	48
O	0	2

Further XRD analysis in Figure 24 shows only a single peak at the 44 degree angle. This is indicative of a single phase being present, and therefore suggests a cobalt-nickel alloy is the only phase in the powder. Had the XRD results shown two distinct peaks around 44 degrees that would suggest a segregated powder containing both nickel

particles and cobalt particles. Instead, the presence of a single peak, in combination with the EDS determined bulk composition; suggest that RES successfully produced a Co-50wt%Ni powder.

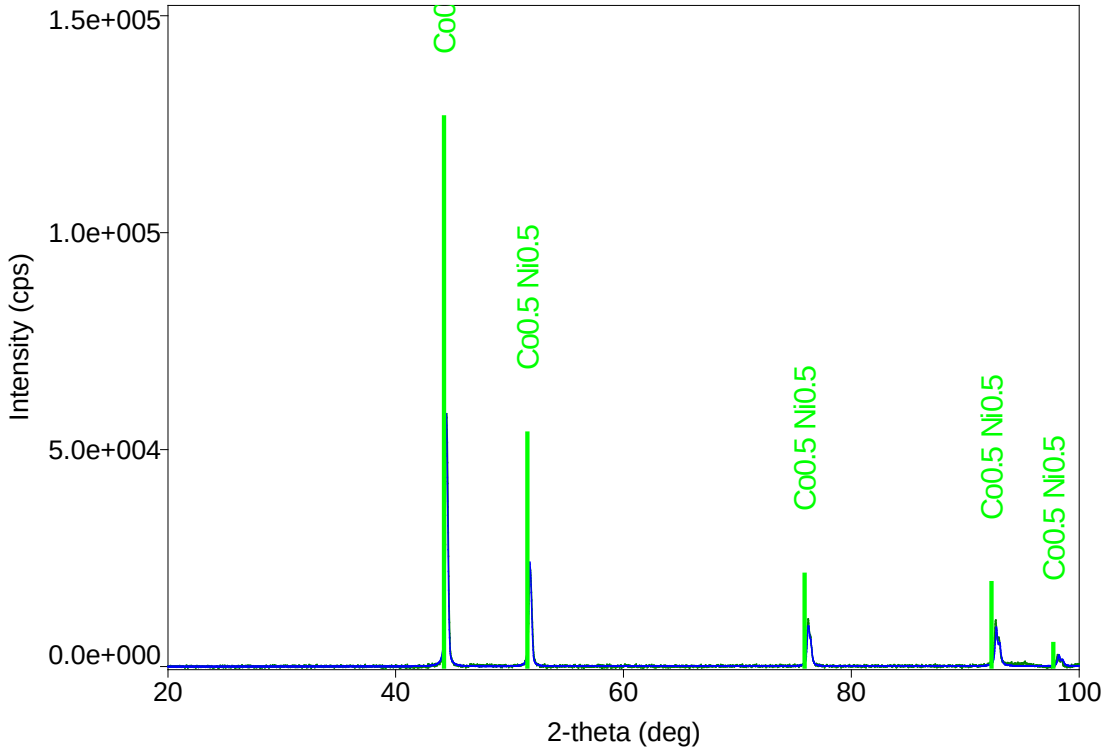

Figure 24. XRD Spectrum for Cobalt-Nickel Powder

d. AlNiCo-5

EDS analysis was used to determine the bulk powder composition of the AlNiCo-5 alloy powder produced using RES. The resulting composition is shown in Table 6. While there is a small amount of oxidation present, the synthesized powder's bulk composition is extremely close to that of AlNiCo-5. However, further analysis of atomic structure through XRD is necessary to ensure that the powder is indeed an alloy rather than a mixture of pure nickel and pure cobalt powders.

Table 6. AlNiCo-5 Powder EDS Results

Element	Wt%	At%
Fe	49	45
Ni	16	14
Al	11	20
Co	25	22

XRD characterization of the AlNiCo-5 alloy powder shows several distinct phases throughout the bulk sample material. The peak at around 36 degrees is associated with aluminum, while the two peaks around 44 degrees are associated with nickel, iron, cobalt, or some combination of those elements, as seen in previous alloys of cobalt-nickel and iron-nickel. The fact that there are two peaks in the 44 degree region suggests two phases were formed. However, extending the width of the XRD analysis to larger angles allows for analysis of the entire XRD pattern. The peaks at both 63 and 82 degrees are characteristic of AlNiCo alloys, as demonstrated in [29]. Thus, it can be concluded that RES is at least partially effective at AlNiCo-5 alloy powder synthesis. The XRD spectrum shown in Figure 25 differs from the other spectra used throughout this thesis due to the fact that the database used for this work does not include an AlNiCo-5 reference card. Therefore, XRD spectrum analysis of the AlNiCo-5 sample was performed by comparing it to the published XRD spectrum in [29].

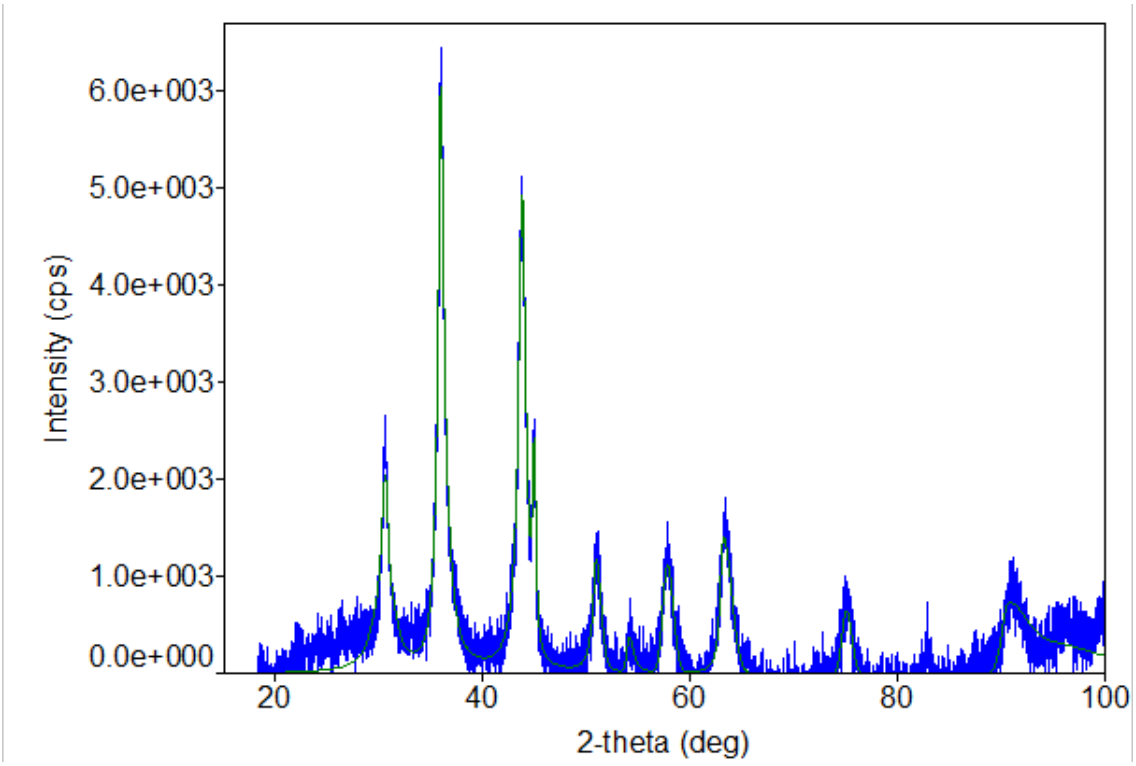

Figure 25. XRD Spectrum for AlNiCo-5 Powder

2. Particle Size Analysis with SEM

In order to analyze each powder's particle size, SEM images were used. The SEM images allowed for the analysis of large quantities of particles and aided in creating a particle size distribution associated with the various ferromagnetic powders.

a. Fe-78wt%Ni

To characterize the particle size distribution and particle morphology associated with the iron-nickel alloy powder, several SEM images were created. First, an effort was made to determine the post-synthesis structure of the "dry" SEM specimens. Figure 26 shows the basic structure of the particles following synthesis. The individual grains of powder can be visually identified, and determined to be on the hundred nm scale.

Figure 26 also allows for characterization of the particle morphology associated with the cobalt-nickel alloy produced via RES. The particles appear to have consistent morphology, and are by and large the same size. This suggests that they should be useful

for 3D printing applications, where a predictable and consistent particle size is essential to maximize the mechanical properties of the printed object.

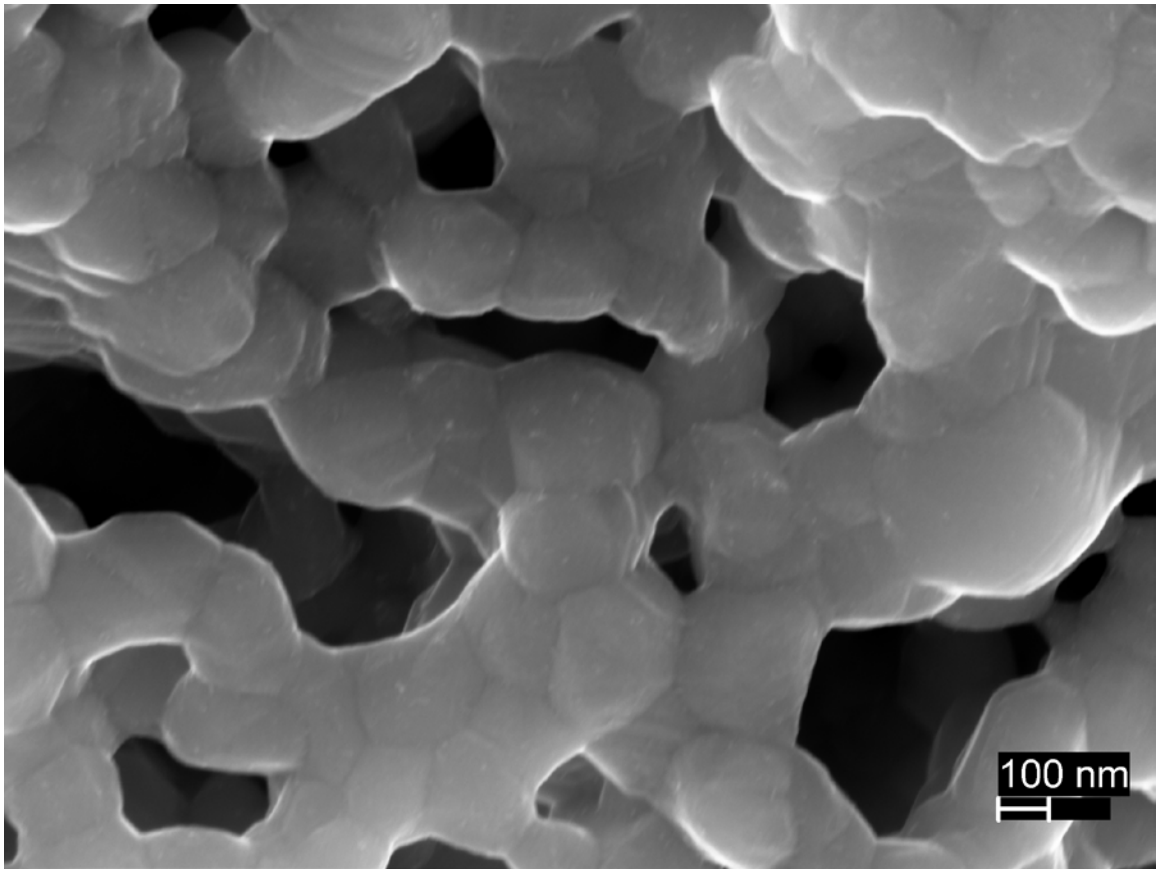

Figure 26. Fe-78wt%Ni Powder in SEM, 50kx Magnification, 20keV

Additional characterization of the particles was conducted using the “wet” samples which were dispersed in ethanol prior to being characterized in the SEM. A dispersed sample’s SEM image is shown in Figure 27. Visually, signs of magnetic agglomeration can be seen in the distribution resulting from the dispersed particles in the “wet” sample. ImageJ was used to create a particle size analysis of the “wet” sample, which was then analyzed in R (an open source statistical analysis software package). Figure 28 is a histogram showing the particle size distribution. The particle size analysis shows a mean particle diameter of 600 nm, and a median value of 450 nm supporting the

conclusion that RES is a useful technique for the manufacture of submicron iron-nickel powders.

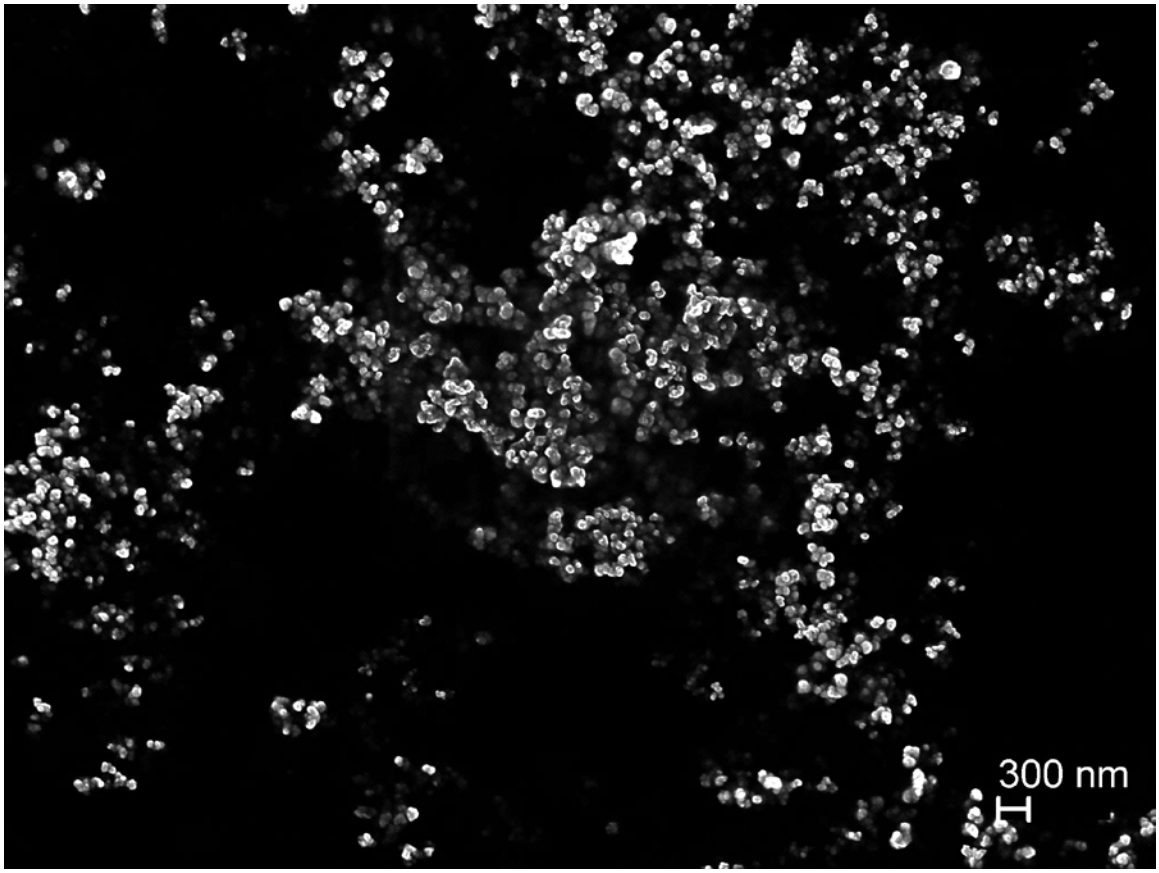

Figure 27. Ni-78wt%Ni Powder Dispersed with Ethanol in SEM, 10kx Magnification, 20keV

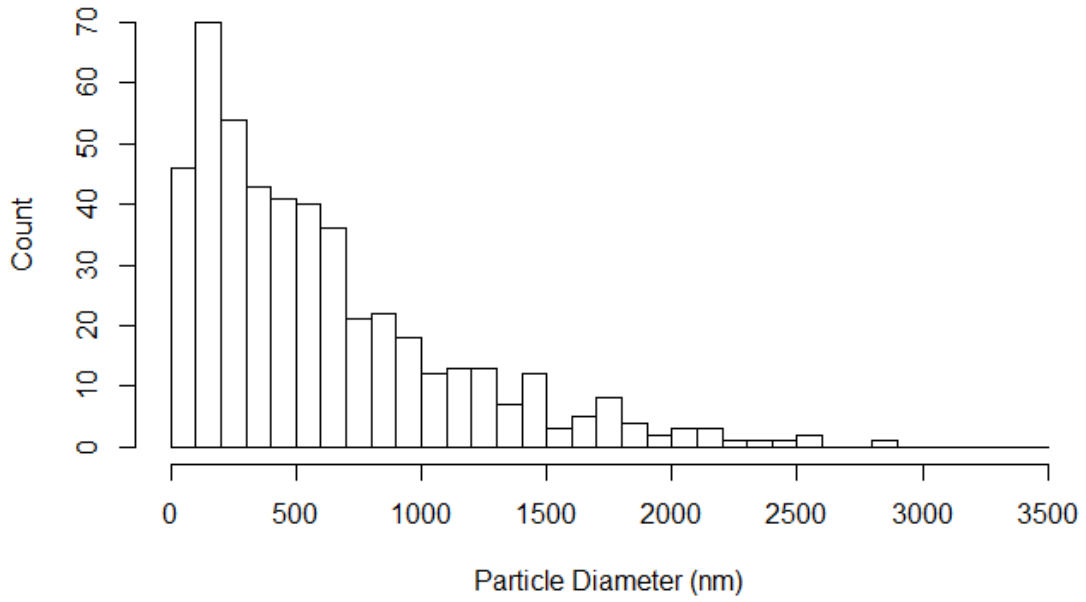

Figure 28. Particle Size Distribution for Fe-78wt%Ni, n=482

b. Fe-50wt%Ni

To characterize the particle size distribution and particle morphology associated with the iron-nickel alloy powder, several SEM images were created. First, an effort was made to determine the post-synthesis structure of the "dry" SEM specimens. Figure 29 shows the basic structure of the particles following synthesis. The individual grains of powder can be visually identified, and determined to be on the hundred nm scale. The smaller (less than 25 nm) particles on the surface of the larger grains are likely residual particles left over from the RES process.

Figure 29 also allows for characterization of the particle morphology associated with the cobalt-nickel alloy produced via RES. The particles appear to have consistent morphology, and are by and large the same size. This suggests that they should be useful for 3D printing applications, where a predictable and consistent particle size is essential to maximize the mechanical properties of the printed object.

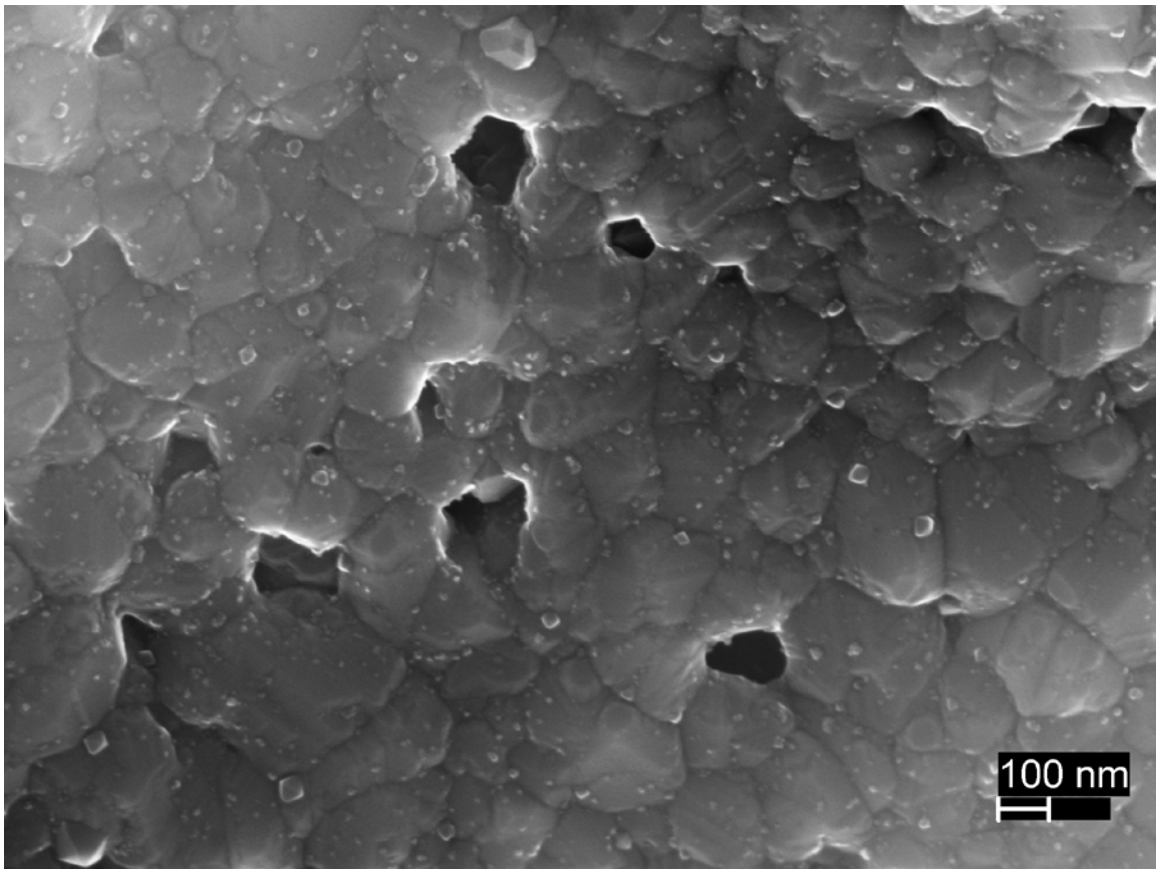

Figure 29. Fe-50wt%Ni Powder in SEM, 50kx Magnification, 20keV

Additional characterization of the particles was conducted using the “wet” samples which were dispersed in ethanol prior to being characterized in the SEM. A dispersed sample’s SEM image is shown in Figure 30. Visually, signs of magnetic agglomeration can be seen in the distribution resulting from the dispersed particles in the “wet” sample. ImageJ was used to create a particle size analysis of the “wet” sample, which was then analyzed in R. Figure 31 is a histogram showing the particle size distribution. The particle size analysis shows the mean particle diameter is 750 nm, and the median diameter is 500 nm, supporting the conclusion that RES is a useful technique for the manufacture of submicron iron-nickel powders.

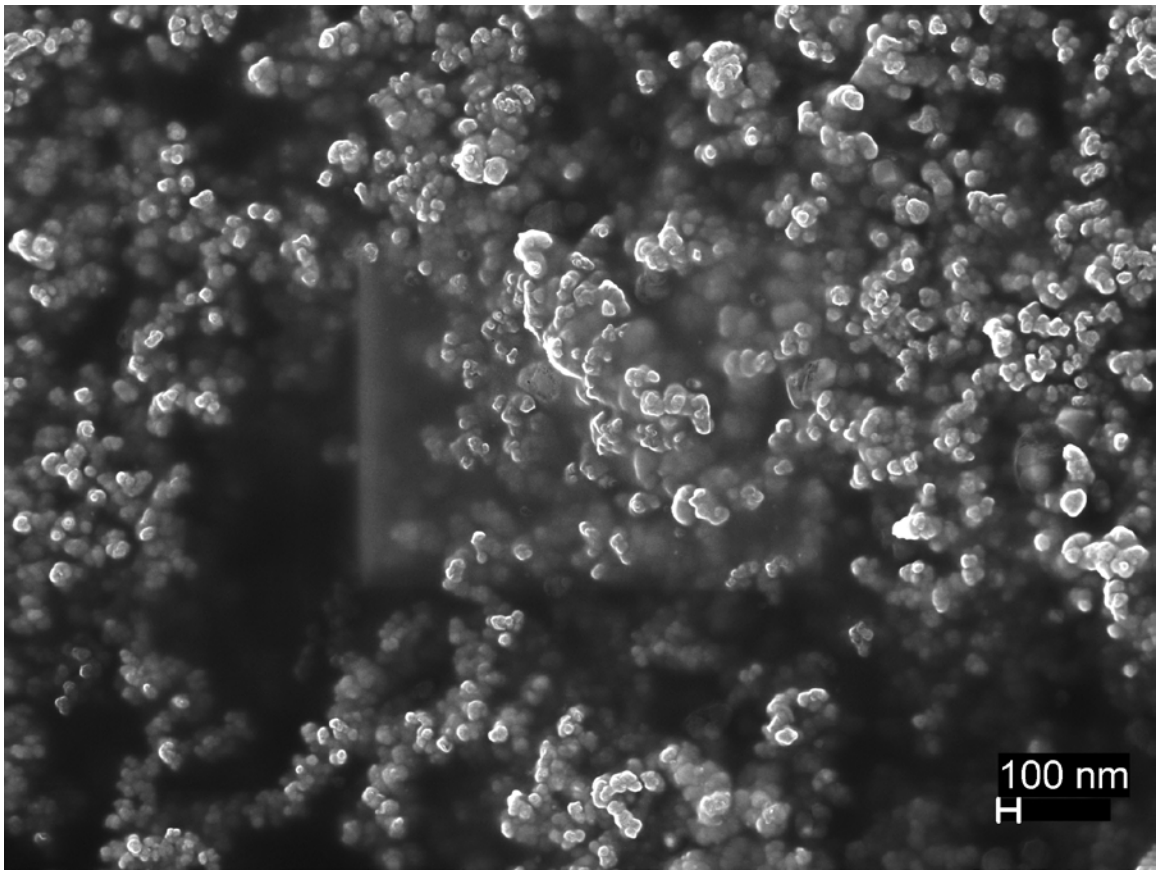

Figure 30. Fe-50wt%Ni Powder Dispersed with Ethanol in SEM, 20kx Magnification, 20keV

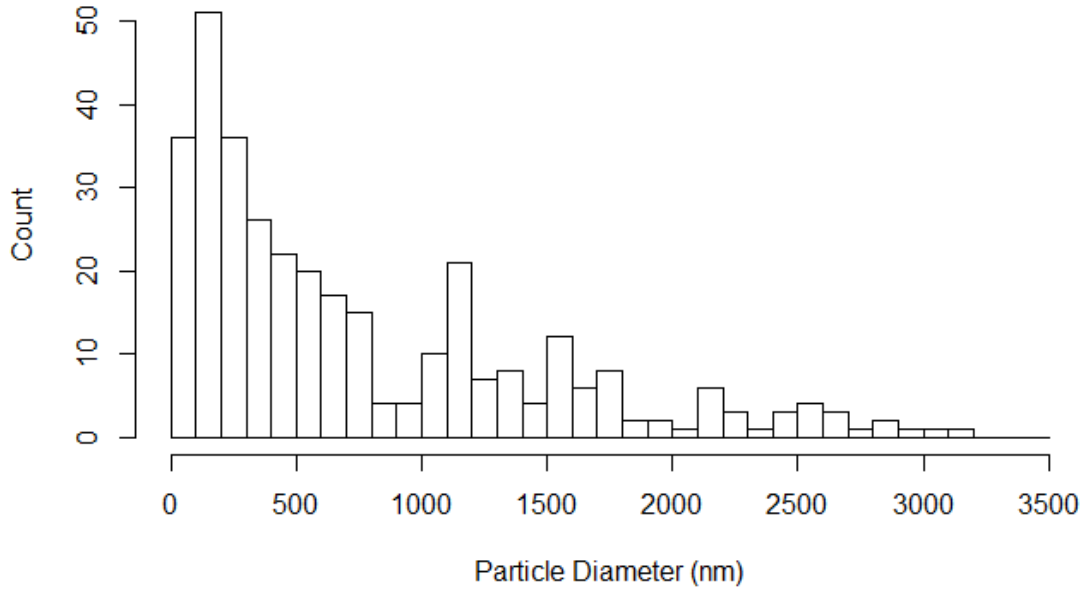

Figure 31. Particle Size Distribution for Fe-50wt%Ni, n=338

c. Co-50wt%Ni

To characterize the particle size distribution and particle morphology associated with the cobalt-nickel alloy powder, several SEM images were created. First, an effort was made to determine the post-synthesis structure of the “dry” SEM specimens. Figure 32 shows the basic structure of the particles following synthesis. The individual grains of powder can be visually identified, and determined to be on the hundred nm scale. The smaller (less than 50 nm) particles on the surface of the larger grains are likely residual particles left over from the RES process.

Figure 32 also allows for characterization of the particle morphology associated with the cobalt-nickel alloy produced via RES. The particles appear to have consistent morphology, and are by and large the same size. This suggests that they should be useful for 3D printing applications, where a predictable and consistent particle size is essential to maximize the mechanical properties of the printed object.

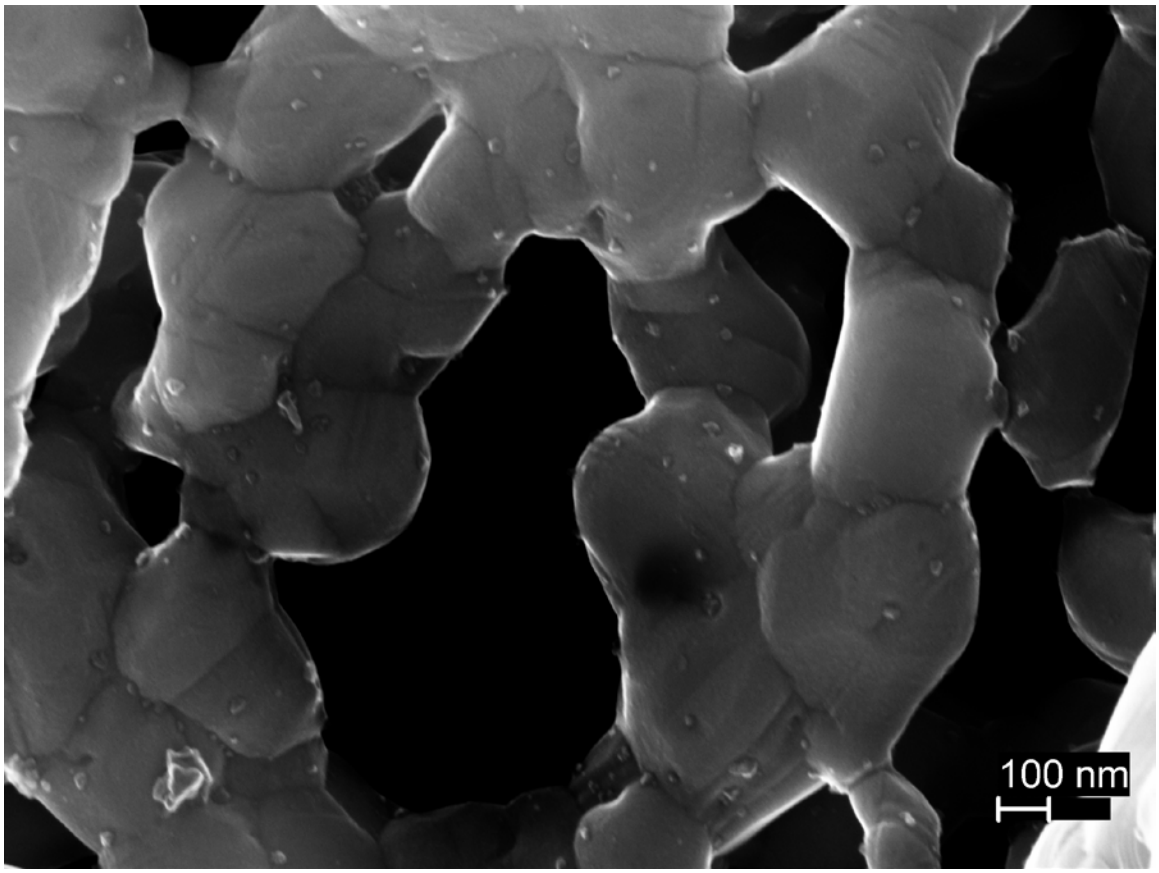

Figure 32. Co-50wt%Ni Powder in SEM, 50kx Magnification, 20keV

Additional characterization of the particles was conducted using the “wet” samples which were dispersed in ethanol prior to being characterized in the SEM. A dispersed sample’s SEM image is shown in Figure 33. Visually, signs of magnetic agglomeration can be seen in the distribution resulting from the dispersed particles in the “wet” sample. ImageJ was used to create a particle size analysis of the “wet” sample, which was then analyzed in R. Figure 34. is a histogram showing the particle size distribution. The particle size analysis shows the mean particle diameter is 750 nm, while the median diameter is 550 nm, supporting the conclusion that RES is a useful technique for the manufacture of submicron cobalt-nickel powders.

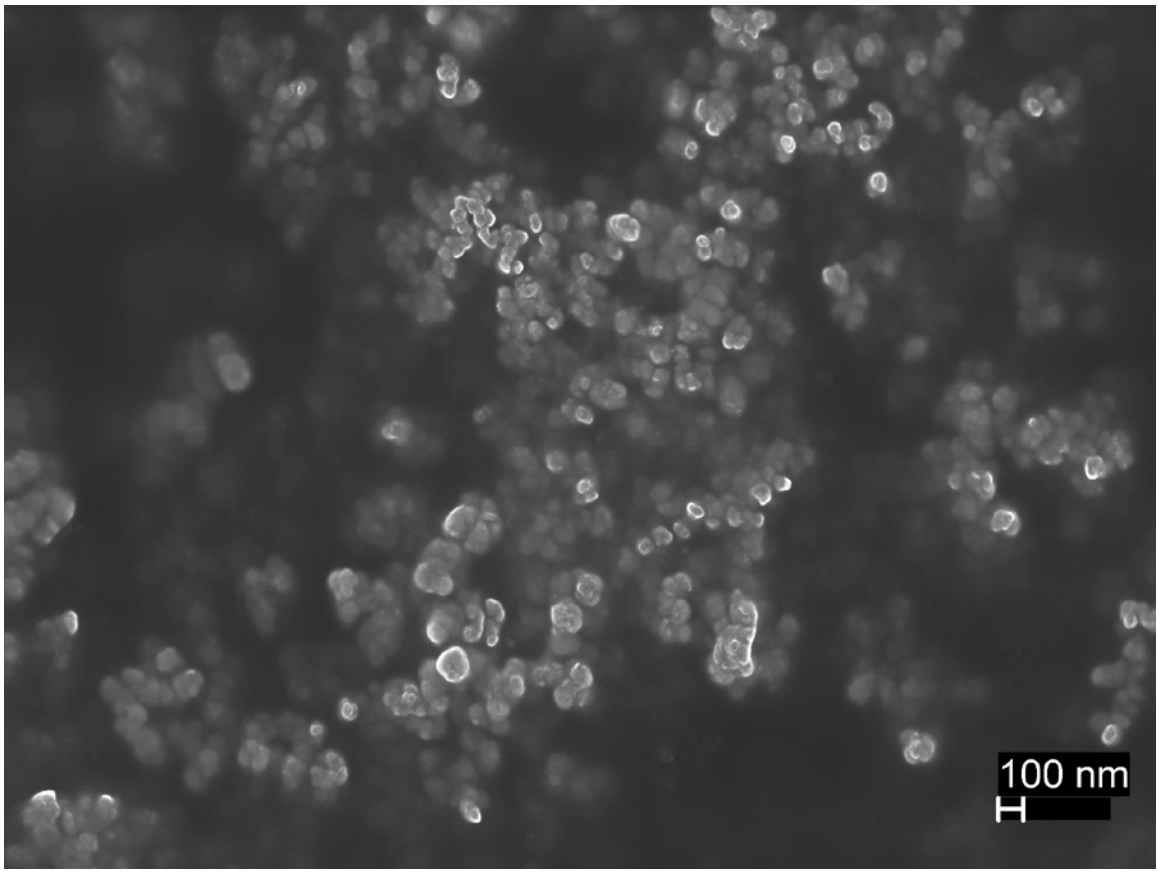

Figure 33. Co-50wt%Ni Powder Dispersed with Ethanol in SEM, 25kx Magnification, 20keV

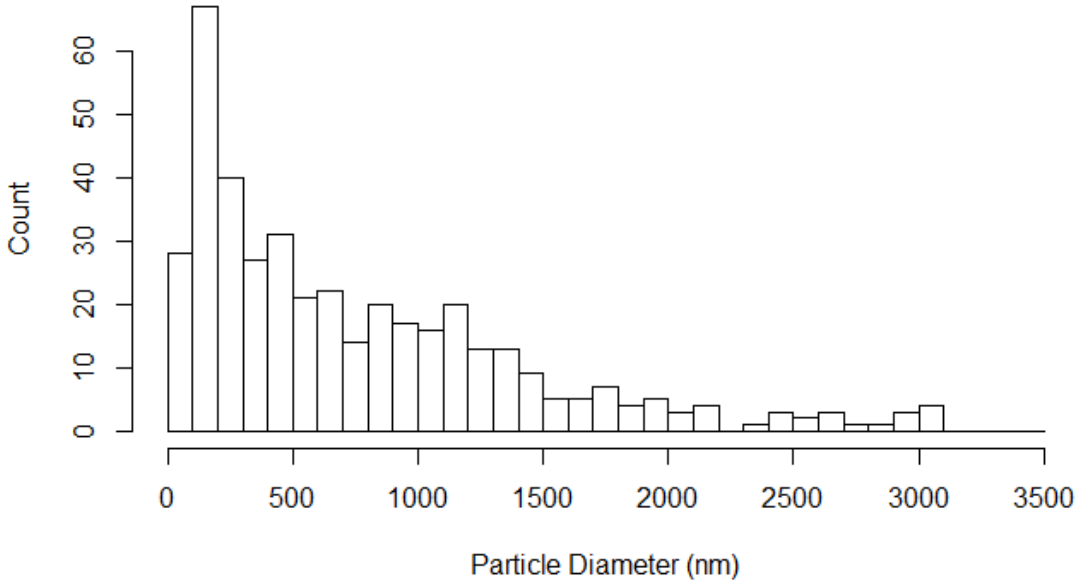

Figure 34. Particle Size Distribution for Co-50wt%Ni, n=409

d. AlNiCo-5

To characterize the particle size distribution and particle morphology associated with the cobalt-nickel alloy powder, several SEM images were created. First, an effort was made to determine the post-synthesis structure of the “dry” SEM specimens. Figure 35. shows the basic structure of the particles following synthesis. The synthesis process appears to have resulted in a somewhat different morphology for the AlNiCo-5 alloy powder when compared to the other ferromagnetic alloy powders. This is likely the result of the addition of aluminum into the alloy. Aluminum has a lower melting point, and as a result decreases the melting point of the alloy itself. This results in the morphology seen in Figure 35, which appears to show the powder having sintered together into larger agglomerations.

Additional analysis of the dispersed powder in Figure 36 suggests that there are portions of the powdered that did not sinter to larger agglomerations. This powder suggests that RES is possible for use with AlNiCo-5 alloy, however additional experimentation would be required to reduce the amount of sintering and create a more consistent powder.

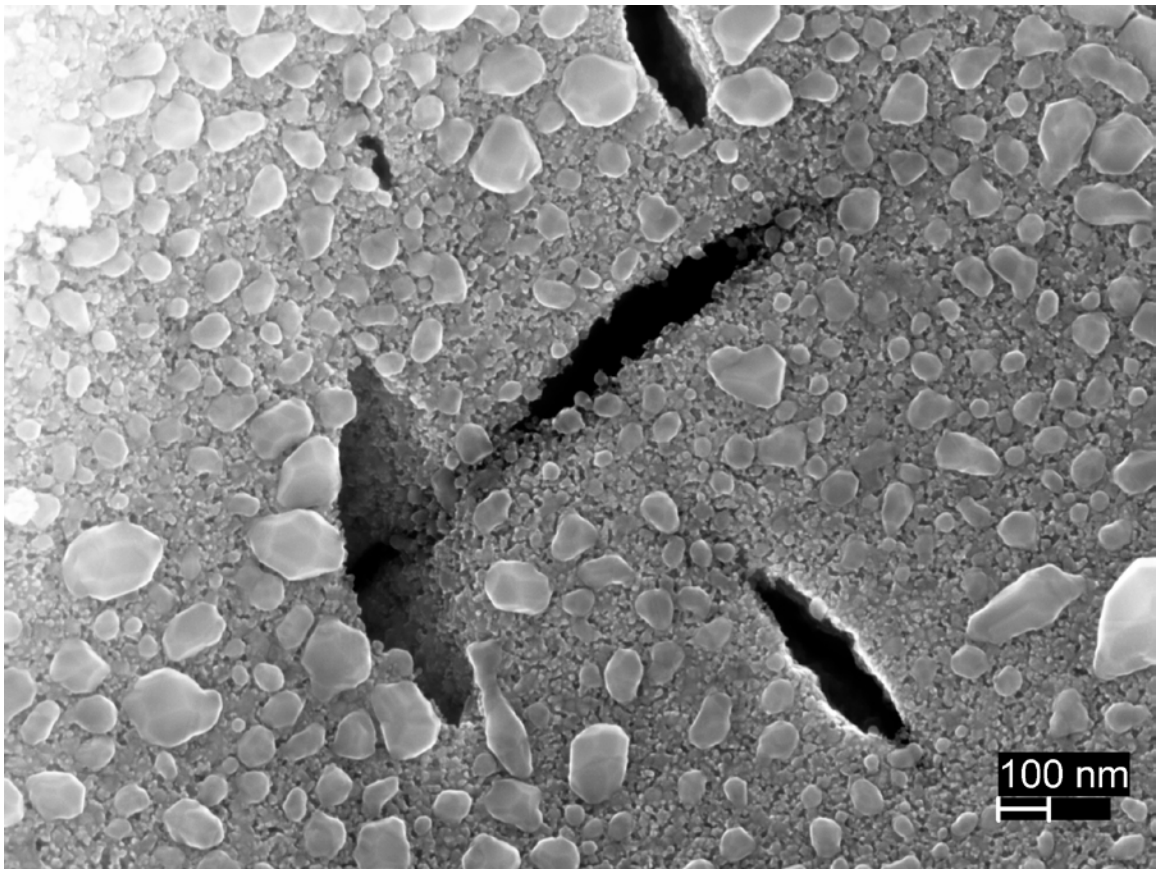

Figure 35. AlNiCo-5 Powder in SEM, 50kx Magnification, 20keV

Additional characterization of the particles was conducted using the “wet” samples which were dispersed in ethanol prior to being characterized in the SEM. A dispersed sample’s SEM image is shown in Figure 36. Visually, signs of magnetic agglomeration can be seen in the distribution resulting from the dispersed particles in the “wet” sample. ImageJ was used to create a particle size analysis of the “wet” sample, which was then analyzed in R. Figure 37 is a histogram showing the particle size distribution. The particle size analysis shows the particles have a mean diameter of 700 nm, and a median diameter of 600 nm, supporting the conclusion that RES is a useful technique for the manufacture of submicron AlNiCo-5 alloy powders. However, this particle analysis fails to adequately describe the bulk of the AlNiCo-5 sample. Due to the large monolithic blocks of sintered powder as seen in Figure 35, the particle size analysis fails to account for the largest particles produced. The process to isolate individual grains used for the particle size analysis does not account for the large blocks, rather it

represents the powder that did not anneal to the bulk sample and was therefore able to be isolated through sonication. Overall, this suggests that there is an additional filtering step required to isolate the useful, submicron, particles produced via RES in an AlNiCo-5 sample. Thus, while the particle size analysis demonstrates that submicron scale AlNiCo-5 alloy powder is readily produced via RES, to truly realize all of the advantages associated with RES, additional work is required to reduce the amount of sintering present on the bulk sample as seen in Figure 35.

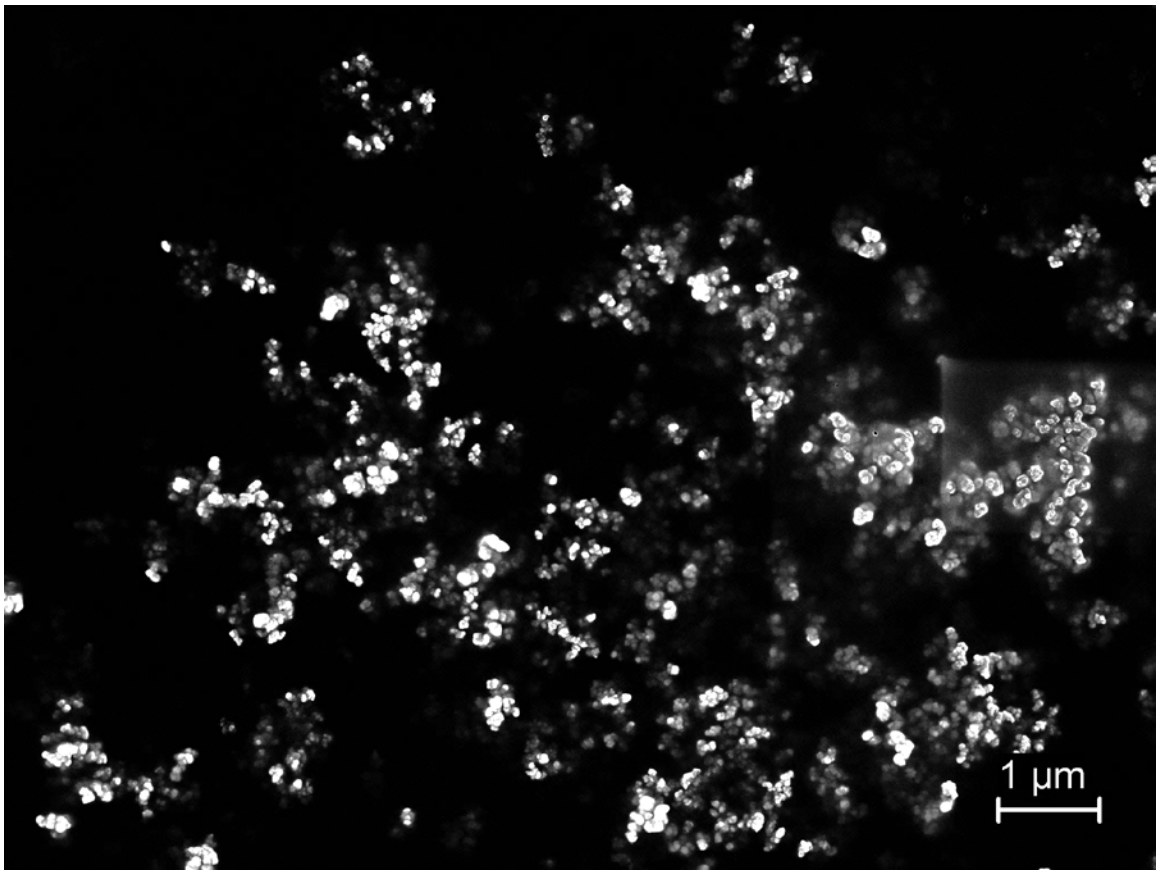

Figure 36. AlNiCo-5 Powder Dispersed with Ethanol in SEM, 10kx Magnification, 20keV

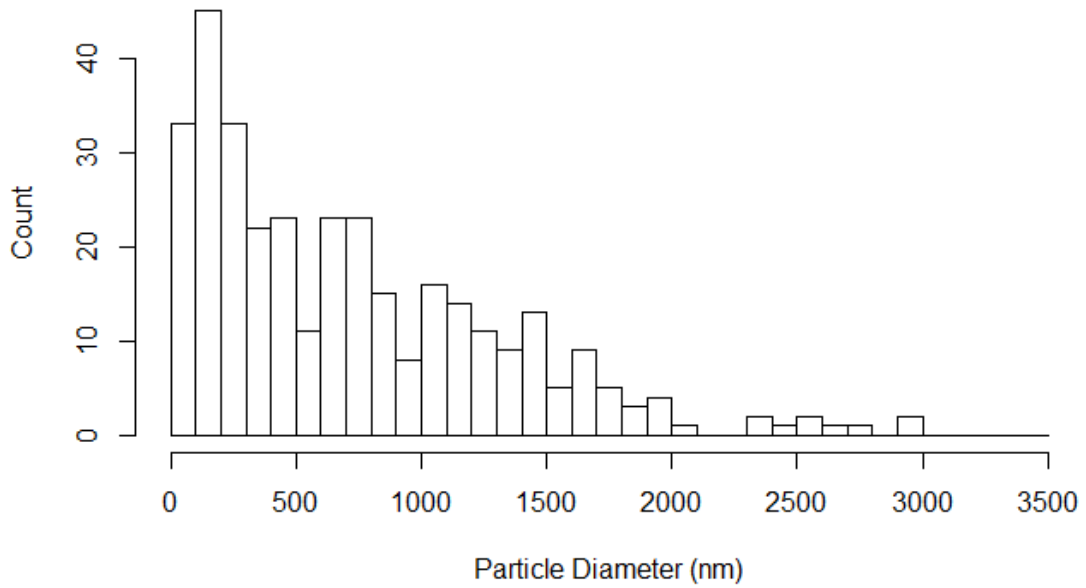

Figure 37. Particle Size Distribution for AlNiCo-5, n=335

3. Discussion of Ferromagnetic Alloy Powder Results

Through the use of various characterization methods, a better understanding of the ferromagnetic alloy powders produced in this thesis was gained. First, XRD and EDS analysis confirmed that the targeted alloy compositions were achieved through RES. Second, the RES generated magnetic particles are consistently smaller than current industry standards. Table 7 summarizes the particle size analysis results to show that all of the ferromagnetic alloy powders produced had grain sizes on the submicron scale. Indeed, the average volume of the particles produced in this work using 600 nm as the average size, is on the order of 5000 times smaller than readily available using standard particle production techniques, Third, given the rapidity of production, the relatively low temperature of the RES process, it is likely a scaled up process will be far less expensive per unit of particle production than present alternatives. For example, “atomization” requires the metal to be heated to the molten state (e.g., Fe melts at 1538 C), which in turn requires special high temperature furnaces and materials. Quite ordinarily materials and furnaces can be employed in the RES process. In any event, cost comparison is

somewhat specious as only RES is capable of making the very small particles required to enable fine feature production using 3D manufacturing or even PIM.

Table 7. Summary of Ferromagnetic Alloy Powder Results

	Particle Diameter (nm)		
Alloy	**Median**	**Mean**	**Standard Deviation**
Fe-50wt%Ni	500	750	700
Fe-78wt%Ni	450	600	500
Co-50wt%Ni	550	750	650
AlNiCo-5	600	700	600

Traditionally, particle size analyses have produced a log-normal distribution of particle diameters [12], [36]. However, the distributions plotted in this work appear to have significantly more large particles than a traditional log-normal distribution, likely a result of magnetic agglomeration. That is the “tail” of the distribution toward larger particles is clearly far longer than normally observed.

The shapes of particle size distributions are often employed as evidence of the dominant growth mode. For example, a log-normal distribution with a sigma value of ca. 1.2 or so is generally understood to result from agglomerating through thermal sintering. Other mechanisms of particle growth produce dramatically different particle size distributions. For example, as discussed elsewhere [36], [37], Ostwald Ripening will create size distributions in which the mean and mode are near the largest particle sizes in the distribution, and the “tail” is on the small size end. Hence, the existence of the distribution observed in the present work, which is loosely “log normal” but with a far larger sigma parameter suggests that some process other than simple thermal agglomeration and growth is at work [36], [38], [39]. The most likely candidate is “magnetic agglomeration.” This type of agglomeration results from the strong magnetic force, particularly in hard magnets, that exists between particles [32]. In sum, probably both thermal agglomeration/sintering and magnetic agglomeration are taking place in the samples produced for this study.

Additionally, it was demonstrated that RES can be effectively "tuned" to a specific alloy composition via precursor selection. This represents a step forward, not only in the field of magnetic powder synthesis, but also for the synthesis of a variety of other metal alloy powders, which can now be manufactured on the submicron scale using RES.

B. MAGNETIC RARE EARTH ALLOY POWDER SYNTHESIS

The effort to synthesize magnetic rare earth metal alloys consisted entirely of trying to create samarium cobalt rare earth magnets. There are two chemical formulas associated with samarium cobalt magnets, $SmCo_5$ and Sm_2Co_{17}. Due to the fact that the weight compositions of both alloys are very close to one another, as seen in Table 8, there was uncertainty as to which phase RES would produce.

Table 8. Target Compositions of Magnetic Rare Earth Alloy Powder Synthesis

Name	wt% Sm	wt% Co
$SmCo_5$	34	66
Sm_2Co_{17}	23	77

1. Composition Determination with EDS and XRD

Several samarium cobalt samples were produced, with precursor compositions determined by Table 1. The precursor ratios were selected so that $SmCo_5$ was the target samarium cobalt phase. EDS analysis of the bulk powder material produced through RES suggested the compositions described in Table 9. The weight percentages are very close to the desired ratio from Table 8; however ,XRD analysis is also needed prior to concluding whether or not $SmCo_5$ was successfully synthesized.

Table 9. Samarium-Cobalt Powder EDS Results

Element	Wt%	At%
Sm	36	18
Co	64	82

XRD analysis of the produced powder produced the spectrum shown in Figure 38. The spectrum suggests two materials were created, Sm_2Co_{17} and samarium oxide. The peaks at 36 and 44 degrees are characteristic of Sm_2Co_{17}, while the peaks at 33,47, and 51 degrees is associated with Sm_2O_3 an oxidized form of samarium. This suggests that RES is capable of producing the desired samarium-cobalt alloy; however, the synthesis technique is not as effective with the Lanthanide series samarium as it is with a transition metal element. This results in the production of a substantial amount of pure samarium which then oxidizes after exposure to air.

By knowing the specific phases formed by RES for the samarium-cobalt alloy, it is possible to determine the total fraction of samarium that formed Sm_2Co_{17} relative to the total sample. Using the bulk sample EDS results, stoichiometry shows that 53% of the Samarium was used for the formation of the Sm_2Co_{17} while the remainder formed pure samarium which later oxidized when exposed to air.

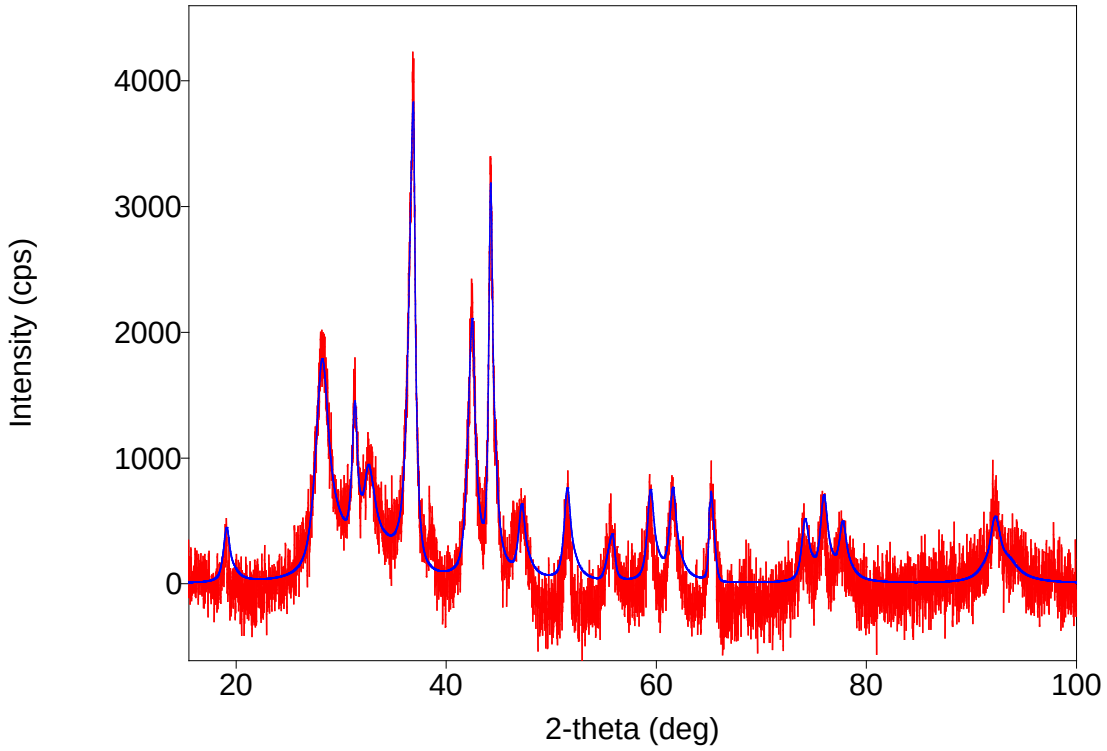

Figure 38. XRD Spectrum for Samarium-Cobalt Powder

Additional work was done to characterize the composition of an individual powder grain in order to confirm the XRD results. This was done using EDS with the STEM feature of the TEM. Figure 39 shows a homogeneous distribution of samarium and cobalt atoms throughout an individual particle, with no evidence of phase separation. The oxygen atoms seen in the figure are a result of oxidation after RES, a result that appears to be more prevalent in the samarium-cobalt powders than the various ferromagnetic alloy powders.

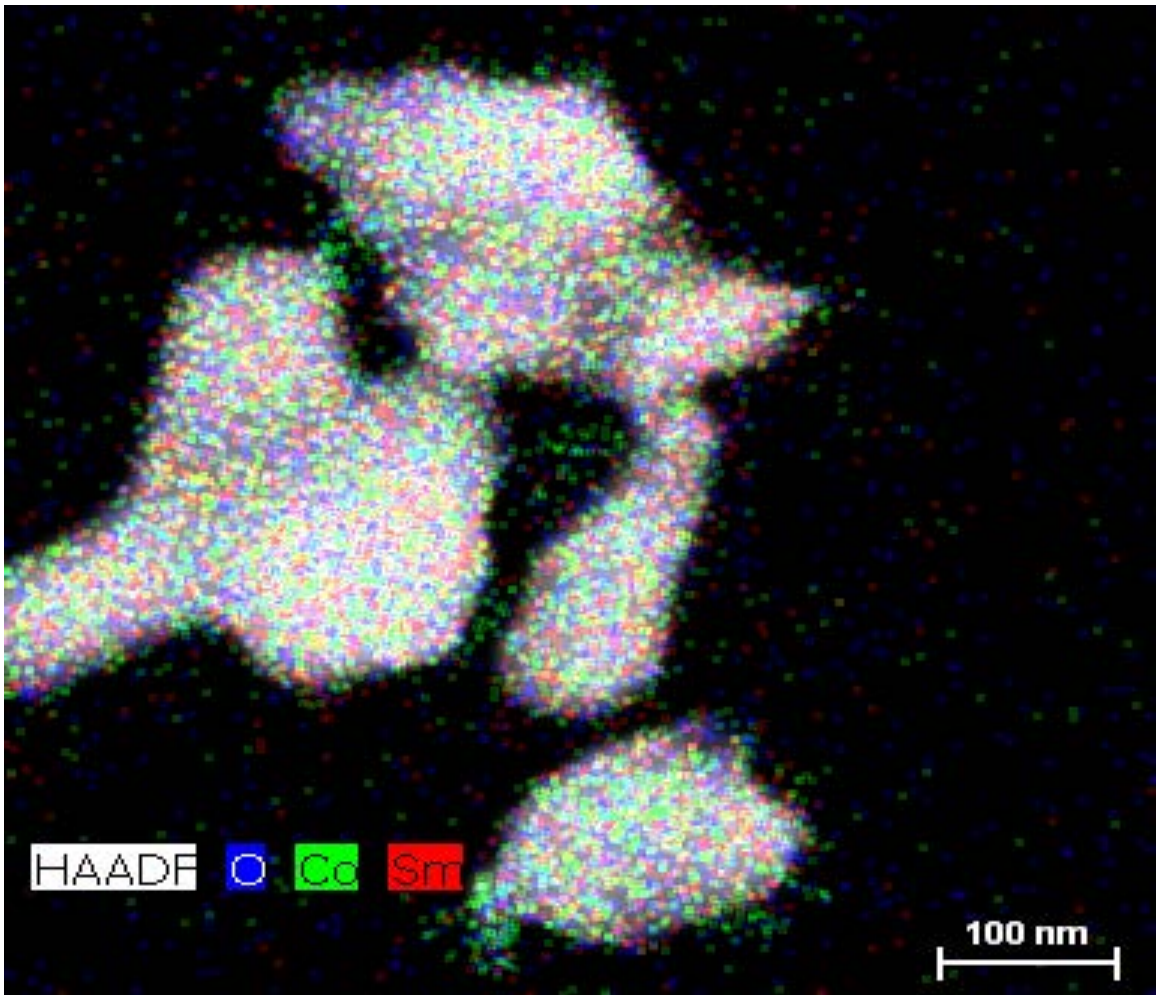

Figure 39. STEM Image of Samarium-Cobalt Powder Particle with EDS Color Mapping

2. Particle Size Analysis with SEM

To characterize the particle size distribution and particle morphology associated with the cobalt-nickel alloy powder, several SEM images were created. First, an effort was made to determine the post-synthesis structure of the “dry” SEM specimens. Figure 40. shows the basic structure of the particles following synthesis. The individual grains of powder can be visually identified, and determined to be on the hundred nm scale.

Figure 40 also allows for characterization of the particle morphology associated with the cobalt-nickel alloy produced via RES. The particles appear to have consistent morphology, and are by and large the same size. This suggests that they should be useful

for 3D printing applications, where a predictable and consistent particle size is essential to maximize the mechanical properties of the printed object.

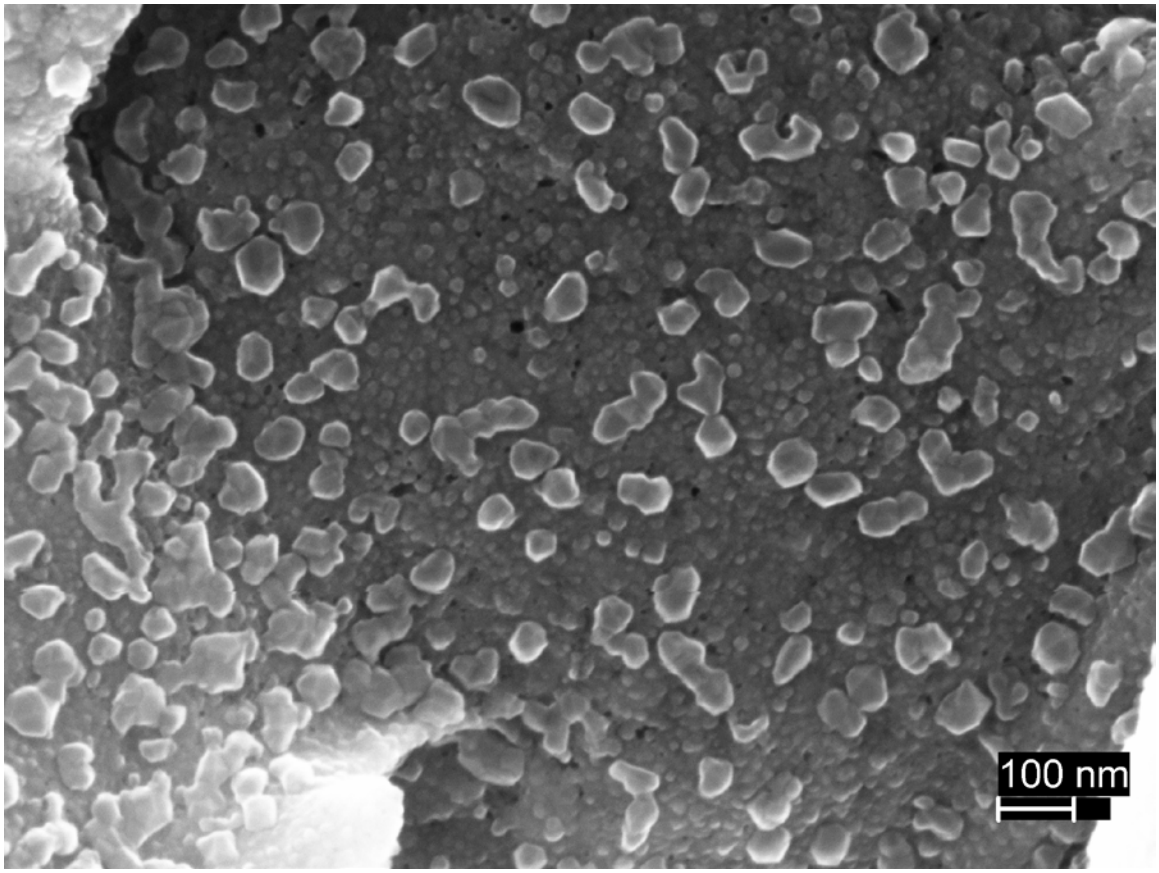

Figure 40. Sm_2Co_{17} Powder in SEM, 75kx Magnification, 20keV

Additional characterization of the particles was conducted using the "wet" samples which were dispersed in ethanol prior to being characterized in the SEM. A dispersed sample's SEM image is shown in Figure 41. Visually, signs of magnetic agglomeration can be seen in the distribution resulting from the dispersed particles in the "wet" sample. ImageJ was used to create a particle size analysis of the "wet" sample, which was then analyzed in R. Figure 42 is a histogram showing the particle size distribution. The particle size analysis shows the particles have a mean diameter of 600 nm, and a median diameter of 400 nm, supporting the conclusion that RES is a useful technique for the manufacture of submicron samarium-cobalt powders.

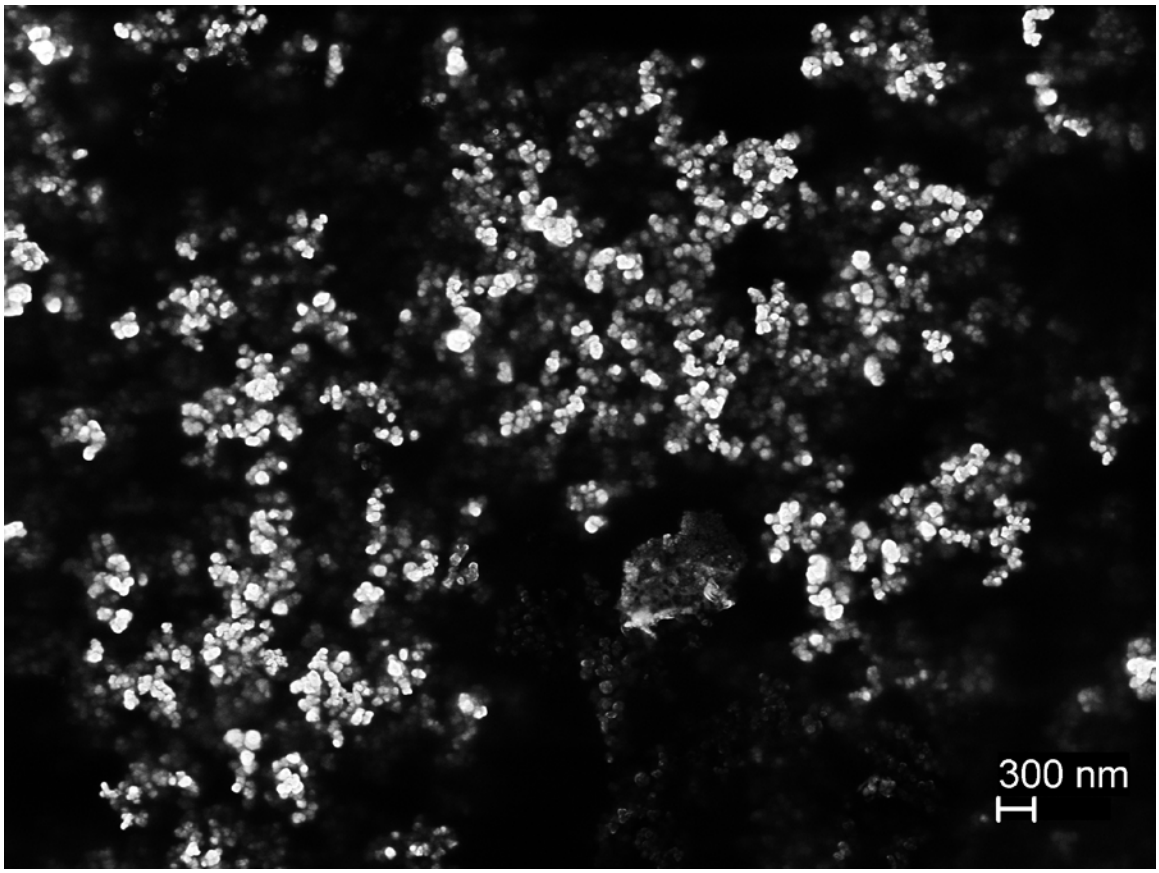

Figure 41. Sm_2Co_{17} Powder Dispersed with Ethanol in SEM, 11.88kx Magnification, 20keV

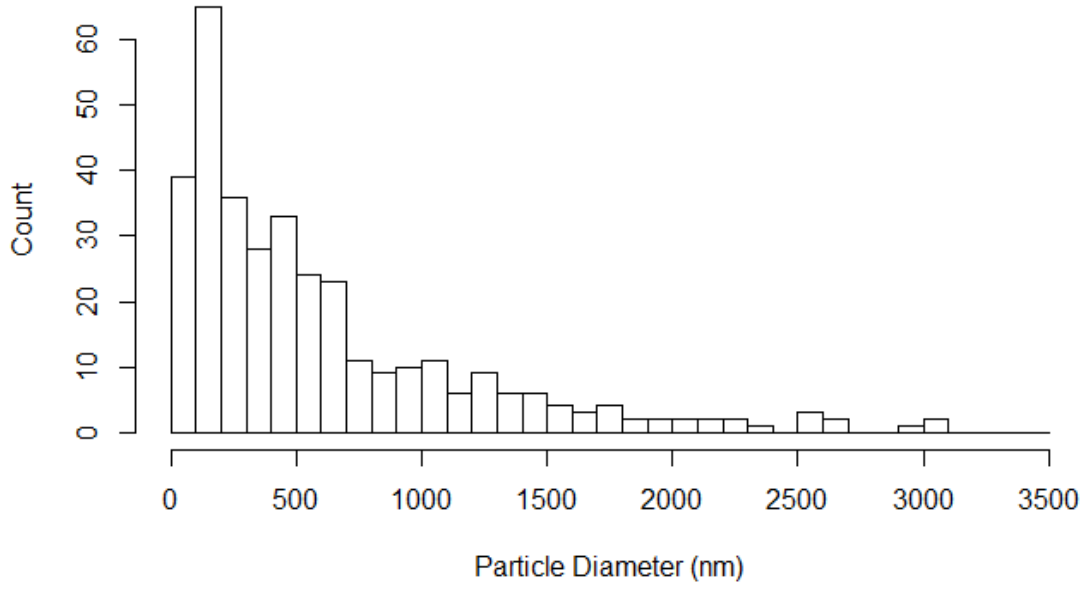

Figure 42. Particle Size Distribution for Sm_2Co_{17}

3. Discussion of Magnetic Rare Earth Alloy Powder Results

By producing magnetic rare earth alloy powders with a submicron grain size, it was demonstrated the RES can be used with Lanthanide series elements such as Samarium. While RES only produced one rare earth alloy powder, with a median grain diameter of 400nm, a mean diameter of 600nm, and a standard deviation of 600nm the result suggests that RES is an alternative to the current energy intensive processes of producing micron scale powders.

As noted above for the iron-nickel particles, traditionally, particle size analyses in which growth by agglomeration is dominant have produced a log-normal distribution of particle diameters [12]. However, just as with the iron-nickel particles the distributions plotted in this work appear to have significantly larger particles than a traditional log-normal distribution. As discussed above, this is likely a result of magnetic agglomeration.

While only Sm_2Co_{17} powder was produced, it is still believed that other samarium-cobalt alloys could be produced through modifications to the precursor ratios. However, due to the lack of experimental evidence, this thesis did not demonstrate the capability to “tune” the alloy composition of a Lanthanide series element through precursor selection.

V. CONCLUSIONS

This section explores the Results in terms of the initial goals of this thesis. The potential use of both ferromagnetic powders and magnetic rare earth alloy powders produced using RES is discussed in terms of applicability to both 3D metal printing and Metal Injection Molding.

A. FERROMAGNETIC POWDER SYNTHESIS

The objective of this thesis in terms of *ferromagnetic powder synthesis* was to use RES to create various alloy powders, representing both hard and soft magnets. The thesis intended to create soft magnet alloys of both iron-nickel, and cobalt-nickel, for use in various military and industrial applications. The thesis also sought to synthesize a hard magnetic AlNiCo alloy using the RES technique.

The RES technique was successfully applied to the soft magnetic alloys as confirmed by a combination of EDS, SEM, and XRD. The EDS and XRD confirmed that not only were all alloying constituents successfully reduced, but that also the desired phase of the alloy was synthesized. This suggests that when working with cobalt, nickel, and iron RES is highly effective at achieving a desired alloy composition through the proper selection of precursors as described in the experimental methods chapter. The SEM enabled further particle size analysis which showed an average particle size of less than a micron, thus achieving the submicron particle size goal. While the specific size of particle varied based on alloy composition, within a specific compositions the size distribution was narrow. This suggests that RES may be applied to further synthesis of submicron soft magnetic particles for 3D printing or MIM applications, as the resulting product is both predictable and consistent.

Applying RES to the creation of a hard magnet showed somewhat promising results. The EDS and XRD analysis confirmed successful synthesis of AlNiCo-5 alloy, the SEM results were mixed in terms of their promise. The particle size analysis suggested that AlNiCo-5 particles had formed on the submicron scale. However, the bulk AlNiCo-5 sample had sintered into large agglomerations on the hundred micron scale.

This result suggests that the current experimental techniques used for RES must be adjusted to account for the presence of low melting temperature species. Although the target alloy itself may have a melting temperature far in excess of that reached during the RES process, the specific elements may not.

The formation of large sintered agglomerates of AlNiCo suggests a model for alloy formation during RES. Unlike all the other species employed in the present work (Fe, Ni, Co, Sm) aluminum has a melting temperature (660 C) below that employed in the RES process. The unusual sintering observed for RES particles produced using aluminum, suggests this general process:

1) At the first stage of the RES process, that is during the initial attack on oxygen by reducing radical species produced by urea decomposition, elements are produced in a pure state. This is a reasonable postulate as the precursors are not ‘alloyed’. Next, there are two possible next steps, depending on the melting temperature of the elements in the alloy.

2 a) In the case of alloys composed of metals that melt above the RES process temperature, alloys subsequently form by interdiffusion of atomic species. Only solid phases are present at all times.

2 b) In the event that an element with a melting temperature below that of the RES process, such as aluminum, is present, alloys may form by a combination of interdiffusion and bulk, liquid phase, flow. This ‘flow’ process would lead to the creation of large particles before the final alloy phase formed and froze. Thus, the formation of sub-micron metal particles using RES with metals that melt below the process temperature may be difficult. Certainly more complex, but still standard, metal processing techniques, such as quenching, may be required.

Still, the particle sizes for the AlNiCo are compatible with the current state of the art for metal 3D printing, or MIM. However, the current synthesis methods would likely prove incapable of producing only submicron particles without the requirement for additional filtering and sorting steps, which would likely reduce the economic advantage created by RES.

B. MAGNETIC RARE EARTH ALLOY POWDER SYNTHESIS

The second objective of this thesis was to apply RES to the production of samarium-cobalt magnetic powders. As there were two separate phases of samarium-cobalt that were extremely similar in terms of mass fraction compositions, there was uncertainty in terms of which phase would be produced. There was additional uncertainty in terms of how successfully RES could be applied to a Lanthanide series element (samarium).

By using precursor mass fractions more closely associated with $SmCo_5$, it was expected that $SmCo_5$ would be the resulting product. EDS and XRD analysis showed that the actual final product was a combination of Sm_2Co_{17} and samarium-cobalt oxide. The excess cobalt and samarium present, from the precursor measurements designed to produce the other phase of samarium-cobalt, was converted to the samarium-cobalt oxide. Additional TEM analysis showed that the samarium-cobalt had formed a homogeneous alloy on the individual particle level of analysis. SEM particle size analysis showed that the samarium-cobalt powder was produced on a sub-micron level. Taken together, these results suggest that RES is a suitable technique to synthesize magnetic rare earth alloys for use in 3D printing and MIM applications.

C. OVERALL SUCCESS

The objective of this thesis was to demonstrate the RES could be used to produce small grain size magnetic alloy powders for use in 3D printing and MIM. By successfully synthesizing four distinct ferromagnetic alloys and one magnetic rare-earth alloy powder, all with an average grain size on the submicron scale, the main objective was met. Table 10. offers a comparison of the powders produced in this thesis with those produced by current industrial processes, as well as lab processes (the processes which have only been performed in a lab and not on the industrial scale are marked with “(lab)”) not only is the overall energy cost reduced by utilizing RES, but also the average grain size is also decreased by a factor of no less than ten when compared to the techniques currently used in industry. This reduction in particle size should allow for the successful manufacture of smaller 3D metal printed and MIM parts than previously possible.

Table 10. Comparison of RES to industrial methods

Method	**Particle Size (μm)**	**Source**
RES (lab)	<1	[10, 17, 18] (and this thesis)
Jet Milling	37	[14]
Jet Milling (lab)	4	[9]
Atomization	10	[13]
BASF Carbonyl Method	2	[15]
Reduction in Hydrogen (lab)	<1	[16]

VI. RECOMMENDATIONS FOR FUTURE WORK

As presented in the Conclusions, this thesis demonstrated success in producing submicron scale magnetic powders of both ferromagnetic alloys and rare-earth alloys. From this foundation, several different opportunities are available to expand on this study. They include additional testing, prototyping of large-scale operations, and application of the powders in a variety of modern component production methods.

A. REDUCTION EXPANSION SYNTHESIS SCALE-UP

It has been demonstrated in this thesis as well as in [17] and [10] that RES is a useful means of powder synthesis for a variety of metals on the bench scale. In particular, it was shown in this thesis that RES, a simple and rapid process, which uses ordinary electric furnaces at relatively modest temperatures (e.g., 800 C) can produce micron and sub-micron sized magnetic particles of a variety of compositions. In contrast, alternative commercial processes, for example atomization, require far higher temperatures (e.g., 1400 C) and specialty equipment, yet can only produce metal particle distributions in which the average particle is thousands of times larger by volume than those produced by RES. Moreover, all indications suggest that RES can be scaled up to produce very large batches of micron and submicron scale particles at a low cost. In particular it is recommended that thorough experimentation on RES scale up be conducted.

B. METAL INJECTION MOLDING APPLICATION

While the powder has been quantitatively shown to be conducive to MIM applications, this thesis did not fabricate any MIM components using the powders produced. It is recommended that a partnership be established for the purposes of testing the use of RES generated particles in a MIM process.

C. 3D PRINTING APPLICATION

While the powder has been quantitatively shown to be conducive to 3D printing applications, this thesis did not fabricate any 3D printed components using the powders produced. All three forms of 3D metal printing should be capable of using the powders

produced through RES in this thesis. A successful demonstration of a 3D printed magnetic component using the powder produced for this thesis would be a highly effective demonstration of RES' usefulness. It is recommended that a partnership be established for the purposes of testing the use of RES generated particles in a 3D printing process.

D. MAGNETIC TESTING

Using a superconducting quantum interference device, the magnetic properties of the powders produced in this thesis could be characterized. By measuring the magnetic characteristics of particles produced using RES, it can be determined whether or not the particles meet the industry standards set by larger particles produced via traditional methods. Should the RES powder perform at the industrial standard level, then it will offer a new economical approach to the production of magnetic components.

LIST OF REFERENCES

[1] M. Cox, “Mobile labs build on-the-spot combat solutions,” *Military. Com*, Aug.17, 2012.

[2] 5965-00-876-2375 loudspeaker, permanent magnet. Available: http://headsetsandmicrophones.tpub.com/11/00-876-2375.htm

[3] *SINCGARS* installation kits component listings. Available: http://vehicularradios.tpub.com/SB-11-131-2/SB-11-131-20040.htm

[4] S. Freedberg, “Navy warship is taking 3d printer to sea; Don’t expect a revolution,” Apr. 22, 2014.

[5] Navy Electricity and Electronics Training Series (NEETS), Module 17, 1-1 to 1-10 - RF Cafe. Available: http://www.rfcafe.com/references/electrical/NEETS-Modules/NEETS-Module-17-1-1-1-10.htm

[6] J. Greenert, J. Amos, and R. Mabus, “Department of the Navy (DON) objectives for fiscal year 2015 (FY15),” Sep. 15, 2014.

[7] R. M. German, H. Wiesner, and R. G. Cornwall, *Powder Injection Molding Technologies: Proceedings of PIM98.* State College, PA 649 Belmont Circle, State College 16803: Innovative Material Solutions, 1998.

[8] D. D. Gu, W. Meiners, K. Wissenbach, and R. Poprawe, “Laser additive manufacturing of metallic components: materials, processes and mechanisms,” *Int. Mater. Rev.*, vol. 57, pp. 133–164, May, 2012.

[9] T. Hartwig, L. Lopes, P. Wendhausen, and N. Unal, “Metal Injection Molding (MIM) of NdFeB magnets,” *The European Physical Journal.Web of Conferences: Proceedings*, vol. 75, pp. 04002-1–4, 2014.

[10] C. Luhrs, M. Kane, Z. Leseman and J. Phillips, “Novel process for solid state reduction of metal oxides and hydroxides,” *Metall. Mater. Trans. B-Proc. Metall. Mater. Proc. Sci.*, vol. 44, pp. 115–122, Feb., 2013.

[11] K. H. Kurth and D. Drummer, “Improvement of the magnetic properties of injection molded polymer bonded magnets,” *2013 3rd International Electric Drives Production Conference (Edpc)*, pp. 7–11, 2013.

[12] W. L. McCabe, J. C. Smith and P. Harriott, *Unit Operations of Chemical Engineering.* Boston: McGraw-Hill, 2005.

[13] P. Grant, “Spray forming,” *Prog. Mater. Sci.*, vol. 39, pp. 497–545, 1995.

[14] How Jet Mills Work - The Jet Pulverizer Company. Available: http://www.jetpulverizer.com/how-jet-mills-work.php

[15] Anonymous “Carbonyl iron powder,” BASF, Evans City, PA, USA, 03/2012. 2012.

[16] G. Lee, S. Kwon, and J. Lee, “Annealing effect on microstructure and magnetic properties of flake-shaped agglomerates of Ni-20wt%Fe nanopowder,” *J. Alloys Compounds*, vol. 613, pp. 164–169, Nov. 15, 2014.

[17] H. Zea, C. Luhrs, and J. Phillips, “Production submicron and nano metallic particles via reductive/expansion method,” in *Abstracts of Papers of the American Chemical Society*, 2011.

[18] S. Wakeland, R. Martinez, J. K. Grey and C. C. Luhrs, “Production of graphene from graphite oxide using urea as expansion-reduction agent,” *Carbon*, vol. 48, pp. 3463–3470, Oct., 2010.

[19] E. P. Furlani, *Permanent Magnet and Electromechanical Devices: Materials, Analysis, and Applications /.* San Diego, CA : London : Academic, 2001.

[20] L. Zhou, M. K. Miller, P. Lu, L. Ke, R. Skomski, H. Dillon, Q. Xing, A. Palasyuk, M. R. McCartney, D. J. Smith, S. Constantinides, R. W. McCallum, I. E. Anderson, V. Antropov, and M. J. Kramer, “Architecture and magnetism of alnico,” *Acta Mater.*, vol. 74, pp. 224–233, Aug. 1, 2014.

[21] X. Gao, S. D. Goldstein, A. A. Lin, and R. W. Johnston, “Uv/eb cured integrated magnets-composition and method of fabrication,” Jan. 8th, 2004.

[22] Y. L. Sun, J. T. Zhao, Z. Liu, W. X. Xia, S. M. Zhu, D. Lee, and A. R. Yan, “The phase and microstructure analysis of Alnico magnets with high coercivity,” *J. Magn Magn Mater.* vol. 379, pp. 58–62, Apr. 1, 2015.

[23] R. Heidenreich and E. Nesbitt, “Physical Structure and Magnetic Anisotropy of Alnico 5 .1.” *J. Appl. Phys.*, vol. 23, pp. 352–365, 1952.

[24] B. Gehrmann, “Nickel-iron alloys with special soft magnetic properties for specific applications,” *J Magn Magn Mater.* vol. 290, pp. 1419–1422, Apr., 2005.

[25] Samarium-Cobalt (SmCo) - Goudsmit Magnetic Supplies. Available: http://www.goudsmitmagnets.com/en/permanent-magnets/8-samarium-cobalt-sm-co.html

[26] Y. Li, X. L. Zhang, R. Qiu, and Y. S. Kang, “Synthesis and investigation of SMCo5 magnetic nanoparticles,” *Colloid Surf. A-Physicochem. Eng. Asp.* vol. 313, pp. 621-624, FEB 1, 2008.

[27] S. J. Shin, Y. H. Kim, H. G. Cha, C. W. Kim, Y. S. Kang, and Y. J. Kim, "The synthesis and characterization of SmCo magnetic nanoparticle by thermal decomposition," *Mol. Cryst. Liquid Cryst.*, vol. 464, pp. 621-631, Mar., 2007.

[28] *In situ Microtomography Study of Metallic Powder Sintering*. Available: http://www.esrf.eu/UsersAndScience/Publications/Highlights/2002/Materials/MAT3

[29] X. Li, A. Chiba, M. Sato, and S. Takahashi, "Synthesis and characterization of nanoparticles of Alnico alloys," *Acta Mater.*, vol. 51, pp. 5593–5600, Oct. 20, 2003.

[30] E. A. Peterson and D. A. Krueger, "Reversible, Field-Induced Agglomeration in Magnetic Colloids," *J. Colloid Interface Sci.*, vol. 62, pp. 24–34, 1977.

[31] E. W. C. Lim and R. Feng, "Agglomeration of magnetic nanoparticles," *J. Chem. Phys.*, vol. 136, pp. 124109, Mar. 28, 2012.

[32] K. Sano and M. Doi, "Theory of Agglomeration of Ferromagnetic Particles in Magnetic Fluids," *J. Phys. Soc. Jpn.*, vol. 52, pp. 2810-2815, 1983.

[33] E. Gaffet, M. Tachikart, O. ElKedim, and R. Rahouadj, "Nanostructural materials formation by mechanical alloying: Morphologic analysis based on transmission and scanning electron microscopic observations," *Mater Charact*, vol. 36, pp. 185–190, Apr.-Jun., 1996.

[34] C. Igathinathane, L. O. Pordesimo, E. P. Columbus, W. D. Batchelor and S. R. Methuku, "Shape identification and particles size distribution from basic shape parameters using ImageJ," *Comput. Electron. Agric.*, vol. 63, pp. 168–182, Oct., 2008.

[35] Anonymous "Particle Size Analysis SOP," *Dune Sciences, Inc.*, 2011.

[36] C. Granqvist and R. Buhrman, "Ultrafine Metal Particles," *J. Appl. Phys.*, vol. 47, pp. 2200–2219, 1976.

[37] J. Phillips, Y. Chen and J. Dumesic, "Characterization of Supported Iron-Oxide Particles using Mossbauer-Spectroscopy and Magnetic-Susceptibility," *ACS Symp. Ser.*, vol. 288, pp. 518–533, 1985.

[38] R. Buhrman and C. Granqvist, "Log-Normal Size Distributions from Magnetization Measurements on Small Superconducting Al Particles," *J. Appl. Phys.*, vol. 47, pp. 2220–2222, 1976.

[39] C. Granqvist and R. Buhrman, "Log-Normal Size Distributions of Ultrafine Metal Particles," *Solid State Commun.*, vol. 18, pp. 123–126, 1976.

THIS PAGE INTENTIONALLY LEFT BLANK

INITIAL DISTRIBUTION LIST

1. Defense Technical Information Center
   Ft. Belvoir, Virginia

2. Dudley Knox Library
   Naval Postgraduate School
   Monterey, California